ICK is essential for cell type-specific ciliogenesis and the regulation of ciliary transport

Running title: ICK regulates protein transport at ciliary tips

Taro Chaya[1,2,4,5], Yoshihiro Omori[1,2,3,4], Ryusuke Kuwahara[6], Takahisa Furukawa[1,2,4,*]

[1]Laboratory for Molecular and Developmental Biology, Institute for Protein Research, Osaka University, [2]JST, CREST, [3]JST, PRESTO, 3-2 Yamadaoka, Suita, Osaka, 565-0871, Japan
[4]Department of Developmental Biology, Osaka Bioscience Institute, 6-2-4 Furuedai, Suita, Osaka, 565-0874, Japan
[5]Kyoto University Graduate School of Medicine, Yoshida Konoe-cho, Sakyo-ku, Kyoto, 606-8501, Japan
[6]Research Center for Ultrahigh Voltage Electron Microscopy, Osaka University, 7-1 Mihogaoka, Ibaraki, Osaka, 567-0047, Japan

Key words: ciliary transport; ciliogenesis; kinase; kinesin

Corresponding author:
[*]Author for correspondence
E-mail: takahisa.furukawa@protein.osaka-u.ac.jp
Laboratory for Molecular and Developmental Biology
Institute for Protein Research
Osaka University
3-2 Yamadaoka, Suita, Osaka, 565-0871, Japan
Phone: +81-6-6879-8631
Fax: +81-6-6879-8633

Character count: 60881

Abstract

Cilia and flagella are formed and maintained by intraflagellar transport (IFT) and play important roles in sensing and moving across species. At the distal tip of the cilia/flagella, IFT complexes turn around to switch from anterograde to retrograde transport, however, the underlying regulatory mechanism is unclear. Here, we identified ICK kinase localization at the tip of cilia as a regulator of ciliary transport. In *ICK*-deficient mice, we found ciliary defects in neuronal progenitor cells with Hedgehog signal defects. *ICK*-deficient cells formed cilia with mislocalized Hedgehog signaling components. Loss of *ICK* caused the accumulation of IFT-A, IFT-B, and BBSome components at the ciliary tips. In contrast, overexpression of ICK induced the strong accumulation of IFT-B but not IFT-A or BBSome components at ciliary tips. In addition, ICK directly phosphorylated Kif3a, while inhibition of this Kif3a phosphorylation affected ciliary formation. Our results suggest that ICK is a Kif3a kinase and essential for proper ciliogenesis in development by regulating ciliary transport at the tip of cilia.

Introduction

Cilia are microtubule-based organelles that extend from the surface of various types of cells in vertebrates (Fliegauf *et al.*, 2007; Gerdes *et al.*, 2009; Nigg and Raff, 2009). Upon cell differentiation, some types of cells change their ciliary function by altering their protein components and morphology. For example, neuronal progenitor cells possess short cilia that contain components of Sonic hedgehog (Shh) signaling such as Smo and Gli. Cilia are known to be important for Shh signal transduction (Huangfu and Anderson, 2005). In the absence of Shh pathway stimulation, Smo rarely localizes in the cilia. In this condition, low levels of Gli transcription factors localize to the tip of cilia. However, Shh pathway stimulation induces the accumulation of Smo and Gli in the cilia, and then triggers the transcription of target genes (Corbit *et al.*, 2005; Haycraft *et al.*, 2005; Kim *et al.*, 2009). In the developing central nervous system (CNS), Shh signaling in the cilia plays an essential role for neuronal progenitor cell proliferation and differentiation (Chizhikov *et al.*, 2007; Breunig *et al.*, 2008; Han *et al.*, 2008; Spassky *et al.*, 2008; Willaredt *et al.*, 2008; Besse *et al.*, 2011). In contrast, mature neurons in the adult brain develop long primary cilia, on which several types of G-protein coupled receptors (GPCRs) for neurotransmitters such as melanin-concentrating hormone and somatostatin are localized (Bishop *et al.*, 2007; Berbari *et al.*, 2008; Arellano *et al.*, 2012). Although cilia are morphologically and functionally diverse among different cells as observed in CNS development, the regulatory mechanisms underlying such cell type-specific ciliogenesis are almost unknown.

Cilia are formed and maintained by the evolutionarily conserved process called intraflagellar transport (IFT), the bidirectional protein trafficking of IFT particles along ciliary microtubules. The IFT particles are composed of two subcomplexes called IFT-A

and IFT-B. Anterograde transport of these particles is driven by Kinesin-2, whereas retrograde transport is mediated by cytoplasmic Dynein-2 (Rosenbaum and Witman, 2002). Anterograde transport is switched to retrograde transport at the ciliary tip, where axonemal tubulins are turned over (Ishikawa and Marshall, 2011). In *Chlamydomonas* and *C. elegans*, IFT-A and IFT-B dissociate after reaching the ciliary/flagellar tip and then IFT-B reassociates with IFT-A before retrograde transport (Pedersen *et al.*, 2006; Wei *et al.*, 2012). Although the coordinated traffic switching at ciliary tips has been suggested as required for normal ciliary formation and maintenance (Pedersen *et al.*, 2006; Wei *et al.*, 2012), the regulatory mechanisms underlying transport switching at ciliary tips are poorly understood.

Chlamydomonas LF4, *Leishmania* LmxMPK9, *C. elegans* Dyf-5, and mouse Mak belong to the evolutionally conserved MAP kinase subfamily, which negatively regulates ciliary length (Asleson and Lefebvre, 1998; Berman *et al.*, 2003; Bengs *et al.*, 2005; Burghoorn *et al.*, 2007; Omori *et al.*, 2010). By contrast to cell type-specific expression of Mak, another murine ortholog of *Chlamydomonas* LF4, Intestinal Cell Kinase (ICK), shows ubiquitous expression including in the developing CNS (Togawa *et al.*, 2000). It was reported that ICK is a substrate of Cell cycle-related kinase (Ccrk) (Fu *et al.*, 2006). A mutant of *Dyf-18*, the *C. elegans* ortholog of *Ccrk*, occasionally forms long curved cilia (Phirke *et al.*, 2011). Broad-minded (Bromi), which interacts with Ccrk, is required for the formation of proper structure in cilia (Ko *et al.*, 2010). There was a single case report of a novel neonatal lethal recessive disorder with multiple anomalies involving the endocrine, cerebral, and skeletal systems (endocrine-cerebro-osteodysplasia, ECO) with a homozygous missense mutation in human *ICK*, suggesting a key role for ICK in the development of multiple organ system

(Lahiry *et al.*, 2009). However, the exact biological functions of ICK have not yet been elucidated.

In the current study, we generated and analyzed retina- or brain-specific *ICK*-deficient mutant mice as well as conventional *ICK*-deficient mutant mice. These mice showed phenotypes defective in Hedgehog (Hh) signal transduction in multiple organs. Unexpectedly, we found that ICK, which localizes at the tips of cilia, is required for ciliogenesis in neural progenitor cells but not in mature neurons. Disruption of *ICK* leads to the accumulation of both IFT-A and IFT-B particles. *ICK*-deficient MEFs have shortened and stumpy cilia with an accumulation of Shh signaling molecules. Furthermore, overexpression of ICK promoted the localization of IFT-B but not IFT-A components at ciliary tips. We also found that ICK directly phosphorylates Kif3a, a subunit of Kinesin-2, and that Kif3a phosphorylation is required for normal cilia formation *in vivo*. These results suggest that ICK is a Kif3a kinase and required for ciliogenesis by regulating ciliary transport at ciliary tips.

Results

ICK-deficient mice show neonatal lethality with skeletal, lung, and brain abnormalities

We first examined the expression pattern of *ICK* in the developing CNS. We observed that *ICK* mRNA is expressed in the embryonic day 10.5 (E10.5) neural tube and E15.5 brain including the cerebral cortex (Supplementary Figure S1A and B). *ICK* mRNA was detected in ganglion cells and weakly in progenitor cells at E17.5 (Supplementary Figure S1C). We did not detect *ICK* mRNA at postnatal day 3 (P3) or P21 in the retina (Supplementary Figure S1D and E). In the brain, the expression of *ICK* reached its peak at P2 and gradually decreased at later stages (Supplementary Figure S1F).

We generated *ICK*-floxed mice by flanking *ICK* exon 3 with two *loxP* sites (Supplementary Figure S1G and H). We first mated *ICK*-floxed mice with *CAG-Cre* mice, which express Cre recombinase in female germ cells (Sakai and Miyazaki, 1997), and generated conventional *ICK*-deficient ($ICK^{-/-}$) mice. Absence of ICK mRNA and protein expression in the $ICK^{-/-}$ mice was confirmed (Supplementary Figure S2A and B). *Ccrk* mRNA expression was not upregulated in $ICK^{-/-}$ MEFs (Supplementary Figure S2C). We did not detect *Mak* mRNA expression in either $ICK^{+/+}$ or $ICK^{-/-}$ MEFs. $ICK^{+/-}$ mice were viable and fertile, and developed without an obvious phenotypic abnormality. In contrast, $ICK^{-/-}$ mice died around birth probably because of respiratory failure. $ICK^{-/-}$ mice exhibited preaxial polydactyly in both fore and hind limbs (Figure 1A–C). All four limbs were severely shortened in the $ICK^{-/-}$ mice at E18.5 (Figure 1D and E). We found that the lungs of $ICK^{-/-}$ embryos at E17.5 show the normal arrangement of four right lobes and one left lobe, however, the lobes were markedly

smaller than those of wild-type embryos (Supplementary Figure S2D and E). In contrast to the lung abnormality, other organs, including the liver, kidney and adrenal gland, were normally developed at E17.5. We observed round-shaped olfactory bulbs (Supplementary Figure S2F, arrowheads) and enlarged cerebral cortexes in the *ICK*$^{-/-}$ embryos at E17.5 (Supplementary Figure S2G and H). *ICK*$^{-/-}$ embryos showed hydrocephalus (Figure 1F and G). The expression of *Gli1*, a downstream gene of the Shh signaling cascade, decreased in the *ICK*$^{-/-}$ brain (Supplementary Figure S2I).

ICK is required for proper ciliogenesis of neural progenitor cells and embryonic fibroblasts

ICK$^{-/-}$ embryos displayed phenotypes such as defects in cilia formation and/or Hh signaling, therefore we analyzed ciliary formation in *ICK*$^{-/-}$ mice. Since we found morphological malformations of the brain in *ICK*$^{-/-}$ mice at E17.5, we focused on ICK function at an earlier stage in the CNS. At E15.5, neuronal progenitor cells still proliferate in the ventricular zone of the cerebral cortex (Dehay and Kennedy, 2007). We tested whether loss of *ICK* affects ciliary formation of neural progenitors in the E15.5 cerebral cortex. We observed that neural progenitor cells extend the cilia into ventricles in the wild-type brain (Figure 1H and H'), however, we found few cilia in the *ICK*$^{-/-}$ brain (Figure 1I and I'). In contrast, epithelial cilia in the nasal pit were normal in the *ICK*$^{-/-}$ mice (Supplementary Figure S2J–K'). To further investigate the effect of loss of *ICK* on ciliary formation, we observed cilia in the kidney, skin, and intestine at E15.5 (Supplementary Figure S2L–Q). Cilia in the nephric duct exhibited no obvious change between *ICK*$^{+/+}$ and *ICK*$^{-/-}$ embryos (Supplementary Figure S2L and M). We found fewer cilia in the epidermis and dermis of the skin of *ICK*$^{-/-}$ embryos

(Supplementary Figure S2N and O). In addition, there were markedly fewer cilia in the intestinal muscular layers and submucosa of *ICK*$^{-/-}$ mice (Supplementary Figure S2P and Q). These results suggest that ICK is essential for ciliogenesis in a tissue-specific manner.

Loss of genes required for ciliogenesis often causes defects in dorsal-ventral neural tube patterning, which is tightly regulated by the Shh morphogen (Dessaud *et al.*, 2008). We examined the expression patterns of *HNF3B, Shh, Pax6, Pax7, HB9, Nkx2.2, Nkx6.1* and *Islet1/2* at E10.5, however, we did not find any significant differences in their expression patterns between *ICK*$^{-/-}$ and wild-type neural tubes (Supplementary Figure S3A–P). To investigate the ciliary integrity of neural progenitors, we examined cilia in the neural tube by immunohistochemistry. We found that cilia numbers and lengths decrease in the *ICK*$^{-/-}$ neural tube (Supplementary Figure S3Q–T). To analyze the ultrastructure of neural tube cilia, we performed scanning electron microscopic analysis. We found that ciliary length decreases in the *ICK*$^{-/-}$ neural tube (Figure 1J and K). Mutations in *Dync2h1*, which encodes the heavy chain of the cytoplasmic dynein-2 motor, or *Bromi* cause morphological changes in the cilia (Ko *et al.*, 2010; Ocbina *et al.*, 2011). Unlike *Dync2h1* or *bromi* mutants, cilia in the *ICK*$^{-/-}$ neural tube did not show a swollen morphology. Although we observed ciliary defects in the *ICK*$^{-/-}$ neural tube, it may not be severe enough to disrupt neural tube patterning.

To analyze ICK function in ciliogenesis, we examined the cilia in mouse embryonic fibroblasts (MEFs) from *ICK*$^{-/-}$ embryos at E13.5. We generated an anti-ICK antibody and analyzed subcellular localization of ICK in MEFs. We found that ICK is localized at the tips of the cilia in wild-type MEFs (Figure 1L). We confirmed the loss of ICK in *ICK*$^{-/-}$ MEF cilia (Figure 1M). We observed background signals in the cytoplasm of

both *ICK*$^{+/+}$ and *ICK*$^{-/-}$ MEFs (Figure 1L and M). We found that ciliated cells are fewer and the ciliary length is shorter in *ICK*$^{-/-}$ MEFs (Figure 1N–Q; Supplementary Figure S3U–Z). This result suggests that ICK is essential for ciliary elongation, in contrast to the function of an ICK paralog, Mak, which is required for the negative regulation of ciliary length (Omori *et al.*, 2010).

ICK is required for the ciliogenesis of retinal progenitor cells but not for photoreceptor cells

To investigate the *in vivo* function of ICK in the developing retina, we mated the *ICK*-floxed mouse line with the *Dkk3-Cre* transgenic mouse line, in which Cre-mediated recombination begins in almost all retinal progenitors at around E10.5 (Sato *et al.*, 2007). We generated *ICK*$^{flox/flox}$*; Dkk3-Cre*$^{+}$ (*ICK Dkk3* CKO) mice and found that they were viable and fertile. We confirmed almost complete loss of the *ICK* mRNA in the *ICK Dkk3* CKO retina (Supplementary Figure S4A). ICK protein expression was lost in the *ICK Dkk3* CKO retina (Supplementary Figure S4B).

We found that retinal thickness was reduced in *ICK Dkk3* CKO mice compared to control mice at P0 (Supplementary Figure S4C–G). The numbers of proliferating cells decreased in the *ICK Dkk3* CKO retina (Supplementary Figure S4C–F, H and I). We found that the numbers of cilia markedly decreased in the P0 *ICK Dkk3* CKO retinal progenitor cells (Figure 2A–C). It is known that cilia are essential for Hh signal transduction, and that Shh signaling controls cell proliferation of retinal progenitor cells (Corbit *et al.*, 2005; Huangfu and Anderson, 2005; Wang *et al.*, 2005; Sakagami *et al.*, 2009). Decreased cell proliferation of retinal progenitor cells in the *ICK Dkk3* CKO retina is most likely due to the lack of cilia and Shh-signaling in retinal progenitor cells.

To test whether the loss of *ICK* affects photoreceptor cilia formation and maintenance, we immunostained retinal sections from one month-old *ICK Dkk3* CKO mice with ciliary markers. We observed no obvious difference in the number and length of the ciliary axoneme and connecting cilia between control and *ICK Dkk*3 CKO retinas (Supplementary Figure S4J–O). Ciliary localization of Mak was unaltered between control and *ICK Dkk3* CKO photoreceptors (Supplementary Figure S4J–K"). These results suggest that ICK plays an essential role in ciliogenesis in retinal progenitors but is dispensable for ciliary assembly and maintenance in mature photoreceptor cells.

Conditional deletion of *ICK* in the brain causes cerebellar developmental defects

Then, to investigate *ICK* function in the brain after birth, we generated mice with conditional deletion of *ICK* in the brain. We crossed *ICK*-floxed mice with transgenic mice expressing Cre recombinase under the control of the Nestin enhancer in neurons and glia broadly in the brain at E11.5 (Isaka *et al.*, 1999), to generate $ICK^{flox/flox}$*; Nestin-*Cre^{+} (*ICK Nes* CKO) mice. We confirmed that *ICK* mRNA expression level is markedly reduced in the cerebellum, hippocampus, cerebral cortex, and whole brain in *ICK Nes* CKO mice compared to that of the control mice (Supplementary Figure S5A–D). ICK protein expression was lost in the *ICK Nes* CKO brain (Supplementary Figure S5E). *Ccrk* mRNA expression was not upregulated in the *ICK Nes* CKO brain (Supplementary Figure S5F). We did not detect *Mak* mRNA expression in either control or *ICK Nes* CKO brains. At P4, *ICK Nes* CKO and control mice were indistinguishable, however, at the age of one month *ICK Nes* CKO mice exhibit growth retardation, ataxia and tremor (Supplementary Figure S5G).

We first analyzed the *ICK Nes* CKO brain at one month of age. We found that the

cerebella of *ICK Nes* CKO mice are obviously smaller than those of the control mice (Figure 2D). We found that the cerebellar lobes of *ICK Nes* CKO mice were smaller compared to those of the control mice (Figure 2E and F). Similarly, the hippocampal dentate gyrus (DG) was smaller in the *ICK Nes* CKO mice (Figure 2G and H). In contrast to the $ICK^{-/-}$ mice, no expanded ventricle was observed in the *ICK Nes* CKO brain at P21 (Supplementary Figure S5H and I).

In the cerebellum, cells in the external granule cell layer (EGL) proliferate to produce the pool of granule cell precursors (GCPs) during the first two weeks after birth. GCPs migrate internally past the Purkinje cells to form the inner granule cell layer (IGL) (Sotelo, 2004). To investigate the development of the *ICK Nes* CKO cerebellum more precisely, we compared the control cerebellum with the *ICK Nes* CKO cerebellum at P4. We found defective cerebellar foliation in the *ICK Nes* CKO mice (Supplementary Figure S5J and K). At this stage, the EGL of the *ICK Nes* CKO cerebellum is thinner compared to that of control cerebellum (Figure 2I–L). Proliferating cell numbers were markedly reduced in the *ICK Nes* CKO cerebellum (Figure 2I–L; Supplementary Figure S5L and M). Ciliary numbers were significantly smaller in *ICK Nes* CKO mice compared to that of control mice (Figure 2M–O). To test whether Shh signaling is affected in the *ICK Nes* CKO cerebellum, we analyzed the expression of *Gli1*, a downstream gene of the Shh signaling cascade. *Gli1* expression significantly decreased in the *ICK Nes* CKO cerebellum at P4 (Supplementary Figure S5N). These results suggest that the loss of *ICK* causes ciliary loss in EGL cells and abnormal Shh signaling, resulting in reduction of cell proliferation in the EGL in the *ICK Nes* CKO cerebellum.

ICK is required for postnatal DG neurogenesis

In the DG, granule neuron precursors proliferate and differentiate into granule neurons at postnatal stages (Altman and Bayer, 1990; Li and Pleasure, 2005). The small size of the DG suggests a possible defect in the postnatal generation of granule neurons in the *ICK Nes* CKO mice. We found that numbers of proliferating cells decreased in *ICK Nes* CKO mice (Supplementary Figure S5O–T). This observation suggests that the production of new neurons is defective at postnatal stages in the *ICK Nes* CKO DG.

To observe the cilia in granule neuron precursors, we immunostained Ki67 and AC3 in the DG. We found that the number of Ki67-positive cells with AC3-positive cilia was severely reduced in the *ICK Nes* CKO DG (Figure 3A–C). Previously, formation of the primary cilia and Shh signaling were shown to be required for postnatal DG neurogenesis (Breunig *et al.*, 2008; Han *et al.*, 2008). We found that the *Gli1* expression level was significantly reduced in the *ICK Nes* CKO hippocampus (Supplementary Figure S5U). These results suggest that the loss of *ICK* in the hippocampus causes ciliary loss in DG neural progenitor cells and affects neuronal production through the Shh signal cascade. We did not observe any obvious differences in ependymal cell ciliary formation between the P4 control and *ICK Nes* CKO brain (Supplementary Figure S5V and W).

ICK-deficient mature neurons develop cilia

Mature neurons extend cilia to various parts of the brain including the hippocampus and cerebral cortex. Several types of GPCRs including somatostatin receptor 3 (SSTR3) and melanin-concentrating hormone receptor 1 (MCH1R) were found to localize to the neuronal cilia (Handel *et al.*, 1999; Berbari *et al.*, 2008; Marley and von Zastrow, 2010). We investigated the integrity of the neuronal cilia in *ICK Nes* CKO mice. Unexpectedly,

we found that the cilia are normal in the *ICK Nes* CKO DG and cerebral cortex at one month of age (Figure 3D–I).

We examined ciliary localization of GPCRs in mature neurons. We found that MCH1R and SSTR3 are localized properly in the neuronal cilia of the *ICK Nes* CKO cerebral cortex (Figure 3J–K'; Supplementary Figure S5X–Y'). In contrast to the essential role of ICK for neuronal progenitor ciliogenesis, loss of *ICK* does not appear to significantly affect ciliary formation and GPCR localization in mature neurons.

ICK is required for proper ciliary localization of Shh pathway components

Shh pathway components including Smo and Gli localize to the cilia, and ciliary localization of these components depends on stimulation of Shh signaling (Corbit *et al.*, 2005; Haycraft *et al.*, 2005). To investigate whether ICK is involved in the regulatory mechanism of ciliary transport of Shh signaling components, we observed Shh signal-dependent ciliary localization of Smo, Gli2, and Gli3 using the $ICK^{-/-}$ MEF (Figure 4A–J; Supplementary Figure S6A–I). In the absence of Shh pathway stimulation, Smo rarely localized in the wild-type MEF cilia, however, Shh pathway stimulation with treatment of a Smo-binding Shh pathway agonist (SAG) induced Smo accumulation in the cilia (Figure 4A, B and I). In contrast, we often observed accumulation of the Smo signal in the $ICK^{-/-}$ MEF cilia even without Shh pathway stimulation (Figure 4C, D and I). To confirm the abnormal ciliary accumulation of Smo in the $ICK^{-/-}$ MEFs, we co-immunostained Smo with γ-tubulin in the *ICK* mutant MEFs. We observed that Smo signals in the vicinity of the centriole significantly increased in $ICK^{-/-}$ MEFs compared to those in wild-type MEFs in the absence of Shh pathway activation (Supplementary Figure S6A–D). Unexpectedly, we found the Smo signal

displayed on cilia-like structure in the vicinity of centriole in more than 80 % *ICK*$^{-/-}$ MEFs. We found that about 10% of *ICK*$^{-/-}$ MEFs formed acetylated α-tubulin-positive cilia (Figure 1N–P). Since acetylated α-tubulin is a marker for the ciliary axoneme and Smo is a membrane protein, these data suggest that *ICK*$^{-/-}$ MEF cilia have ciliary membrane structures without acetylated α-tubulin-positive microtubules. Although AC3 and Arl13b are ciliary membrane proteins, we observed that about 10% of *ICK*$^{-/-}$ MEFs form AC3-positive cilia and that about 30% of *ICK*$^{-/-}$ MEFs have Arl13b-positive cilia (Supplementary Figure S3U–Z). The transport system for AC3 and Arl13b in cilia may be different from that for Smo.

In wild-type MEFs, low levels of Gli2 and Gli3 were localized at ciliary tips in the absence of Shh pathway stimulation (Figure 4E and J; Supplementary Figure S6E and I). However, after stimulation with SAG, Gli2 and Gli3 accumulated at ciliary tips (Figure 4F and J; Supplementary Figure S6F and I). In contrast, Gli2 and Gli3 were enriched at cilia tips in the *ICK*$^{-/-}$ MEFs either with or without Shh pathway stimulation (Figure 4G, H and J; Supplementary Figure S6G, H and I). Smo signals in the cilia increased in the E10.5 *ICK*$^{-/-}$ neural tube and paraxial mesoderm (Figure 4K–N). *Gli1* expression was significantly down-regulated in *ICK*$^{-/-}$ MEFs compared to that in wild-type MEFs in the presence of Shh pathway stimulation (Supplementary Figure S6J). These results suggest that ICK regulates the ciliary localization of Shh pathway components.

A kinase-dead mutant and an ECO-associated mutant of ICK have a reduced ability to rescue ciliary formation in *ICK*$^{-/-}$ MEFs

To investigate the regulatory mechanisms for ciliary formation by ICK, we performed rescue experiments using *ICK*$^{-/-}$ MEFs. We prepared constructs expressing a

FLAG-tagged full-length wild-type ICK (ICK-WT) or a kinase-dead mutant ICK (ICK-KD) (Figure 5A). The ICK-KD construct was generated by substitution of a lysine residue (K33) with an arginine residue (Xia *et al.*, 2002; Fu *et al.*, 2005). We transfected these constructs into *ICK*$^{-/-}$ MEFs and observed the acetylated-α-tubulin-positive cilia (Figure 5B–E). While ICK-WT rescued ciliary formation in *ICK*$^{-/-}$ MEFs (Figure 5C and E), ICK-KD failed to rescue the cilia in those cells (Figure 5D and E). ICK-WT rescued ciliary length in *ICK*$^{-/-}$ MEFs (Figure 5F). This result shows that the kinase activity of ICK is essential for its function in cilia formation. We observed that ICK-WT localizes at the ciliary tips (Figure 5C). We found that ICK-KD also localizes in the cilia (Figure 5D), suggesting that kinase activity is not required for ciliary localization of ICK.

It was reported that a missense mutation in human *ICK* is associated with a developmental disorder, ECO (Lahiry *et al.*, 2009). This mutation results in an amino acid substitution from arginine to glutamine at residue 272 of human ICK (R272Q). To investigate whether this mutation affects ICK function, we generated constructs expressing a FLAG-tagged full-length wild-type human ICK (hICK-WT) and FLAG-tagged ECO-associated mutant R272Q of human ICK (hICK-ECO) (Figure 5G). We transfected these constructs into NIH3T3 cells and observed the subcellular localization of the FLAG-tagged proteins (Figure 5H–K). We found that hICK-WT localizes to the ciliary tips in 65% cells (Figure 5I and K). In contrast, the human mutant ICK had a significantly decreased efficiency in localizing to the ciliary tips compared to that of WT hICK (17%, Figure 5J and K). We next examined the ability of the WT hICK and the human ECO mutant to rescue the formation of acetylated-α-tubulin-positive cilia in *ICK*$^{-/-}$ MEFs (Figure 5L–O). We found that

hICK-WT effectively rescues ciliary formation in *ICK*$^{-/-}$ MEFs, whereas hICK-ECO inefficiently rescues cilia in those cells (Figure 5M–O). These results suggest that the R272Q mutation in human ICK causes loss of proper ICK localization in the cilia, resulting in a functional defect of ICK in the cilia.

ICK regulates the localization of IFT components at ciliary tips

IFT is required for proper ciliary localization of Shh signaling components. To examine whether loss of *ICK* affects ciliary transport, we immunostained IFT88 (an IFT-B component) and IFT144 (an IFT-A component) in the cilia of *ICK*$^{-/-}$ MEFs. We observed that the level of IFT88 and IFT144 localized at ciliary tips markedly increased in *ICK*$^{-/-}$ MEFs (Figure 6A–E). We next transfected the FLAG-tagged IFT57 (an IFT-B component)-, IFT140 (an IFT-A component)-, or BBS8 (a BBSome component)-expressing plasmids into *ICK*$^{-/-}$ MEFs, and observed the subcellular localization of the FLAG-tagged proteins. These FLAG-tagged proteins were concentrated at ciliary tips in *ICK*$^{-/-}$ MEFs (Figure 6F and G; Supplementary Figure S6K–N). These results show that loss of *ICK* affects IFT machinery. Unlike *Ift122*^{sopb} mutant mice, which show defects in retrograde IFT (Qin *et al.*, 2011), we did not observe an accumulation of IFT88 at the tips of cilia in the *ICK*$^{-/-}$ neural tube at E10.5 (Supplementary Figure S6O–P'). To observe whether overexpression of ICK affects ciliary localization of IFT components, we transfected FLAG-tagged Kif3a, IFT88, IFT57, IFT140, or BBS8 expression constructs with or without the ICK-expressing construct (Figure 6H–V). We found that ICK signals at ciliary tips increase in ICK-overexpressing cells (Supplementary Figure S7A and B). Overexpression of ICK induced slight ciliary elongation (Supplementary Figure S7C–E). IFT88 was distributed

along the ciliary axoneme without the overexpression of ICK (Figure 6L). In this condition, Kif3a, IFT57, and BBS8 rarely localized to the cilia, and IFT140 only slightly localized at the base of the cilia (Figure 6J, N, R, S and U). When ICK was overexpressed, Kif3a, IFT88 and IFT57, but not IFT140 or BBS8, more clearly accumulated at ciliary tips (Figure 6K, M, O, R, T and V). The level of IFT140 localized at ciliary bases increased in ICK-overexpressing cells (Figure 6T). In these cells, IFT88 signals occasionally showed a ring-like structure at the tip of the cilia (Figure 6P and Q). These results show that ICK regulates IFT machinery in the cilia.

Kif3a is phosphorylated by ICK and Kif3a phosphorylation is required for ciliary formation

To identify a phosphorylation target for ICK, we searched for consensus amino acid sequence R-P-X-S/T-P/A/T/S for phosphorylation by ICK in proteins associated with ciliary transport, including components of IFT-A, IFT-B, BBSome, Kinesin, and Dynein motors. We found that Kif3a contains a highly evolutionarily conserved consensus sequence at position 671-675 in its C-terminal region (Figure 7A and B) (Fu *et al.*, 2006). We performed an *in vitro* kinase assay using purified GST-ICK and found that Kif3a-C-WT is markedly phosphorylated by ICK, whereas no obvious phosphorylation of GST alone was detected (Figure 7C). We next generated a construct harboring a Thr-to-Ala mutation at residue 674. We found the phosphorylation level of Kif3a-C-T674A is markedly weaker than that of Kif3a-C-WT (Figure 7C). These results show that ICK directly phosphorylates Kif3a, predominantly at residue 674. To explore whether Kif3a is actually phosphorylated in cells, we made an antibody against phosphorylated Kif3a Thr-674 (p-Kif3a) (Supplementary Figure S8A–C'). We found

that p-Kif3a localizes to the cilia in *ICK*$^{+/+}$ MEFs, and that p-Kif3a signals were often enriched at ciliary bases and tips (Figure 7D). In *ICK*$^{-/-}$ MEFs, the percentage of cilia with p-Kif3a at the ciliary tips markedly decreased (Figure 7E and F). Interestingly, a majority of shortened cilia lost p-Kif3a signals at the tips of cilia (left and middle panels in Figure 7E), whereas cilia of normal length often had p-Kif3a signals at ciliary tips in *ICK*$^{-/-}$ MEFs (right panels in Figure 7E). This result suggests that Kif3a is phosphorylated by ICK at ciliary tips, and that phosphorylation of Kif3a at residue 674 is linked to ciliary formation.

To investigate the role of phosphorylation of Kif3a in ciliary formation, we performed rescue experiments using NIH3T3 cells (Figure 7G–M). We constructed a short hairpin RNA (shRNA) to knockdown *Kif3a* (Supplementary Figure S8D), and found that shKif3a inhibits ciliary formation (Figure 7I and M). Expression of shRNA-resistant Kif3a-WT rescued shKif3a-mediated inhibition of ciliation (Figure 7J and M). Unexpectedly, shRNA-resistant Kif3a-T674A had a slightly increased ability to rescue shKif3a-induced inhibition of ciliary formation compared to that of Kif3a-WT (Figure 7K and M). Since Kif3a-C-T674A was still phosphorylated by ICK (Figure 7C), we thought that phosphorylation of other serine or threonine residues in the C-terminal region of Kif3a may also be important for Kif3a function in ciliary formation. To further analyze the role of phosphorylation of the Kif3a C-terminal region in ciliary formation, we constructed a plasmid encoding the Kif3a mutant in which 8 Ser or Thr residues clustered in the C-terminal region, including residue 674, are replaced with Ala (Kif3a-8xA) (Figure 7G). Expression of shRNA-resistant Kif3a-8xA failed to rescue shKif3a-mediated inhibition of ciliary formation (Figure 7L and M). These results suggest that phosphorylation of the C-terminal region of Kif3a affects ciliary formation

in cultured cells.

To investigate the role of phosphorylation of Kif3a in ciliary formation *in vivo*, we performed rescue experiments using zebrafish embryos. First, *Kif3a* antisense morpholino (Kif3a MO), which was designed to inhibit translation of endogenous *Kif3a*, was injected into zebrafish embryos. At 3 dpf, approximately 60% zebrafish larvae showed a curly body axis, a typical phenotype observed in mutants with ciliary defects (Figure 7N) (Tsujikawa and Malicki, 2004; Omori *et al.*, 2008). In this condition, approximately 30% larvae exhibited severe curly tail phenotype (Figure 7O). In contrast, when we co-injected *in vitro* transcribed wild-type mouse *Kif3a* (Kif3a-WT) mRNA with Kif3a MO, the number of larvae with the curly tail phenotype significantly decreased (Figure 7O). However, when we co-injected Kif3a MO with Kif3a-8xA mRNA, the number of larvae with the curly tail phenotype significantly increased compared to co-injection with Kif3a-WT mRNA.

We also investigated ciliogenesis in the nasal pits of the larvae injected with the morpholino and mRNA (Figure 7P–T). At 3 dpf, cilia have developed in nasal pit epithelia in control larvae (Figure 7P and T). In contrast, larvae injected with Kif3a MO and GFP lost cilia at this stage (Figure 7Q and T). Loss of cilia by Kif3a MO injection was partially rescued by co-injection with Kif3a-WT mRNA (Figure 7R and T). However, co-injection with Kif3a-8xA mRNA failed to rescue the ciliary defect by knockdown of *Kif3a* (Figure 7S and T). Taken together, these results suggest that phosphorylation of the C-terminal portion of Kif3a is essential for normal ciliary formation.

Discussion

Previous studies showed that molecular mechanisms underlying the formation of the cilia are common in most cell types. IFT machinery is essential for the formation of all types of cilia including motile and non-motile (primary) cilia (Louvi and Grove, 2011). For example, a defect of Kif3a causes ciliary loss both in neuronal progenitor cells and mature neurons (Davenport *et al.*, 2007; Spassky *et al.*, 2008). Similarly, ciliary transition zone (TZ) components are also required for the ciliogenesis in many types of cells (Czarnecki and Shah, 2012). Loss of B9d2, a component of the ciliary TZ, causes the defect of the cilia both in neuronal progenitors and neurons in the hippocampus (Breunig *et al.*, 2008). In contrast to the phenotypes of these previously reported mutants, we observed that *ICK* deficiency causes defects only in neural progenitor cells and not in differentiated neurons (Supplementary Figure S8E). This observation suggests that ICK belongs to a new category of factors required for ciliogenesis and that a previously unknown mechanism regulates ciliary assembly in progenitor cells. Why does the loss of *ICK* cause defects in ciliogenesis in neuronal progenitor cells but not in mature neurons? The first possibility is that *ICK* deficiency can be functionally compensated by other ciliary kinase(s) in mature neurons but not in progenitor cells. For example, an ICK paralog, Mak, probably compensates for ICK function in the retinal photoreceptor cells at least. ICK and other kinase(s) may function redundantly in mature neurons. The second hypothesis is that ICK is specifically important for repeating the cycle of formation and reabsorption of the cilia in progenitor cells. Progenitor cells repeatedly assemble and reabsorb cilia during the cell cycle progression. In contrast, mature neurons basically form the cilia only once and never resorb them. Since more IFT activity is probably required for repeated assembly and disassembly of cilia, cilia in

progenitor cells may be more sensitive to a defect of protein transport at ciliary tips than those in mature neurons.

We observed that *ICK*$^{-/-}$ mice display hydrocephalus, whereas *ICK Nes* CKO mice did not. It was recently reported that ciliary defects cause increased apoptosis and impaired proliferation of NG2^{+}PDGFR-α^{+} neural progenitors, resulting in neonatal hydrocephalus (Carter *et al.*, 2012), suggesting that the hydrocephalus observed in *ICK*$^{-/-}$ mice is due to ciliary abnormalities in those progenitors. On the other hand, defects of ependymal cilia cause progressive hydrocephalus at postnatal stages (Tissir *et al.*, 2010). It is known that cilia in ependymal cells are formed after birth (Spassky *et al.*, 2005). We did not observe any obvious differences in ciliary formation of ependymal cells between the P4 control and *ICK Nes* CKO brain. Perinatal hydrocephalus caused by the absence of *ICK* may be compensated for in postnatal development.

A missense mutation in *ICK* was reported in a human ECO patient (Lahiry *et al.*, 2009). The ECO-associated mutant R272Q of human ICK fails to localize at the nucleus and showed diminished kinase activity (Lahiry *et al.*, 2009), however, the molecular mechanism underlying ECO has not yet been elucidated. In our study, we observed that *ICK*$^{-/-}$ mice display neonatal lethality with multiple organ defects including pulmonary hypoplasia, shortened limbs, polydactyly, cerebral cortex malformation, and ventricular hydrocephalus, which is similar to the clinical and pathological features of ECO patients. Thus, our results demonstrate that ICK loss of function causes some of the phenotypes observed in ECO patients. Interestingly, the phenotypes observed in *ICK*$^{-/-}$ mice have similarities with those mutants with defects in cilia formation and/or Hh signaling. Indeed, we showed that ICK is required for proper cilia formation and Hh signaling activity, and that the human ICK R272Q mutant exhibits a diminished efficiency in

localizing to ciliary tips and fails to rescue ciliary formation in *ICK*$^{-/-}$ MEFs. This suggests that ECO is caused by ciliary defects and/or impaired Hh signaling pathway due to ICK dysfunction. *ICK*$^{-/-}$ mice can be useful as a mouse model of human ECO and helpful for understanding the pathogenesis of the disorder.

Our and other studies have revealed that Mak and its homologues negatively regulate ciliary length (Asleson and Lefebvre, 1998; Berman *et al.*, 2003; Bengs *et al.*, 2005; Burghoorn *et al.*, 2007; Omori *et al.*, 2010). Since deficiencies in Mak and its homologues produce elongation of the cilia, we first assumed that loss of ICK exhibits a similar elongated ciliary phenotype. Unexpectedly, we observed shortened and stumpy cilia in *ICK*$^{-/-}$ cells, suggesting that the function of ICK is distinct from that of the previously characterized homologues and paralogues of ICK. The functional difference in ciliary length regulation between Mak and ICK may be due to differences of phosphorylation target specificity, although phosphorylation target specificity is likely to be similar between Mak and ICK because of their well-conserved kinase domains. In contrast to our observations using knockout experiments, a recent study showed that cultured cells knocked down by siRNA against *ICK* exhibit slightly elongated cilia (Yang *et al.*, 2013). This phenotypic difference might be caused by a small amount of ICK remaining in the knocked down cultured cells. We found that shRNA-resistant Kif3a-T674A has a slightly increased ability to rescue shKif3a-induced inhibition of ciliary formation compared to that of Kif3a-WT. Since ciliary numbers decreased in *ICK*$^{-/-}$ cells, we first expected Kif3a-T674A would show reduced ability to rescue shKif3a-induced inhibition of ciliary formation compared to that of Kif3a-WT. The reason why the effect of Kif3a-T674A on ciliary formation in knockdown and rescue experiments using cultured cells is the opposite of the results obtained from *ICK*

knockout experiments is unclear, however, the study by Yang *et al*. reported that knockdown of *ICK* and *Mak* promote ciliary formation in cultured cells (Yang *et al.*, 2013). Suppression of the expression of *ICK* may promote ciliary formation through reducing the level of Kif3a phosphorylation at residue 674 in cultured cells.

How is ICK involved in cilia formation in progenitor cells? Cilia are assembled by IFT, which is divided into anterograde transport powered by Kinesin-2 and retrograde transport driven by cytoplasmic Dynein-2 (Rosenbaum and Witman, 2002). IFT trains turnaround and switch from anterograde to retrograde at the ciliary tip. IFT particles and their cargos dissociate after reaching the ciliary tip and then reorganize for retrograde transport (Pedersen *et al.*, 2006). In this study, using overexpression and knockout experiments, we showed that ICK localizes at ciliary tips and regulates the ciliary transport machinery (Figure 8). A mutation in *Bromi*, which encodes an interaction partner of Ccrk, leads to a swollen or bulbous morphology in cilia (Ko *et al.*, 2010), whereas $ICK^{-/-}$ neural tube cilia do not display that morphology. Although ICK is a substrate of Ccrk (Fu *et al.*, 2006), ICK may have a distinct function from that of Bromi. How does ICK get to ciliary tips? If ICK is transported to ciliary tips by anterograde IFT, the activity of ICK may be suppressed by unknown mechanisms while this protein is being transported as a cargo. This is because proteins that should function at a distinct cellular region must be properly trafficked to that region by Kinesin and play their roles only after arriving.

It was reported that some factors are implicated in the regulation of IFT at ciliary/flagellar tips in invertebrates. In *Chlamydomonas* and *Tetrahymena*, IFT172 is involved in the transport transition between anterograde and retrograde IFT at the tips of cilia and flagella (Pedersen *et al.*, 2005; Tsao and Gorovsky, 2008). The BBSome and

DYF-2 (an orthologue of human IFT144) were reported to cooperate to regulate IFT assembly and turnaround at the ciliary tips in *C. elegans* (Wei *et al.*, 2012). Hypomorphic mutations in *bbs-1* and *dyf-2* cause the specific accumulation of IFT-B components at ciliary tips, which is similar to the phenotype observed in ICK-overexpressing cells. In contrast, both IFT-A and IFT-B components were concentrated at ciliary tips in *ICK*$^{-/-}$ MEFs. ICK may regulate disassembly between IFT-A and IFT-B subcomplexes to prepare for retrograde transport. We also observed that BBS8 is concentrated at ciliary tips in *ICK*$^{-/-}$ MEFs, suggesting that ICK deficiency leads to an excess amount of BBSome at ciliary tips and aberrantly promotes IFT assembly. ICK may control ciliary transport through regulating BBS proteins. To our knowledge, ICK is the only regulatory molecule identified to date that controls transport switching at ciliary tips. How does ICK regulate protein transport at ciliary tips through phosphorylation? We observed that Kif3a is directly phosphorylated by ICK. The phosphorylated form of Kif3a localized to the ciliary tips. The inhibition of phosphorylation of Kif3a affected its function in ciliary formation. Based on these observations, we propose a hypothetical model in which ICK regulates protein transport at the ciliary tips at least partially through phosphorylating Kif3a. Our data on ICK phosphorylation of Kif3a is supported by a previous study showing that loss of function of *Dyf-5*, the *C. elegans* orthologue of *ICK*, affects the function of Kinesin-2 motors in cilia (Burghoorn *et al.*, 2007). Since p-Kif3a signals at ciliary tips did not completely disappear in *ICK*$^{-/-}$ MEFs, ICK may not be the only Kif3a kinase. We observed that Kif3a-8xA more strongly affects ciliary formation than Kif3a-T674A. This observation and the result that Kif3a-C-T674A is still phosphorylated by ICK suggest that ICK regulates Kif3a function through phosphorylation of residue 674 as well as other

residues in the Kif3a C-terminal region. However, we cannot exclude the possibility that other kinases contribute to the phosphorylation of that region of Kif3a. We further suppose that there may be other ICK phosphorylation target proteins playing roles in the regulation of ciliary transport. Future studies will advance our understanding of the detailed mechanisms of protein transport at ciliary tips.

Materials and methods

Generation of *ICK*^{flox} mice

We subcloned a ~12 kb *ICK* genomic fragment, inserted one *loxP* site into intron 2 and another *loxP* site into intron 3, cloned it into a modified *pPNT* vector to make a targeting construct, and transfected the linearized targeting construct into the TC1 embryonic stem (ES) cell line (Deng *et al.*, 1996). The culture, electroporation, and selection of TC1 were performed as described previously (Muranishi *et al.*, 2011). ES cells that were heterozygous for the targeted gene disruption were microinjected into C57BL/6 blastocysts to obtain chimeric mice.

Generation of *ICK* knock-out (KO) mice and *ICK* conditional knock-out (CKO) mice

We mated the *ICK*^{flox} mouse line with a *CAG-Cre* transgenic mouse line, which expresses Cre recombinase under control of the *CAG* promoter, to obtain a null-allele of *ICK* (Sakai and Miyazaki, 1997). We also mated the *ICK*^{flox} mouse line with transgenic mice expressing Cre recombinase under control of the *Nestin* promoter (*Nestin-Cre*) (Isaka *et al.*, 1999) or the *Dkk3* promoter (*Dkk3-Cre*) (Sato *et al.*, 2007).

Antibodies

We used the following primary antibodies for immunostaining: mouse monoclonal anti-acetylated α-tubulin (Sigma, 6-11B-1, 1:1000), anti-Ki67 (BD Pharmigen, 556003, 1:200), anti-Gli3 (gift from Dr. S. J. Scales, 1:1000) (Wen *et al.*, 2010), anti-γ-tubulin (Sigma, GTU-88, 1:300), anti-FLAG-M2 (Sigma, F1804, 1:1000), anti-NeuN

(Millipore, MAB377, 1:500), and anti-polyglutamylated tubulin (Adipogen, GT335, 1:500); mouse polyclonal anti-IFT144 (Abnova, H00057728-B01P, 1:250); rabbit polyclonal anti-AC3 (Santa Cruz, sc-588, 1:300), anti-phospho-histone H3 (Millipore, 06-570, 1:300), anti-Smo (gift from Dr. K. V. Anderson, 1:500) (Ocbina *et al.*, 2011), anti-IFT88 (gift from Dr. G. J. Pazour, 1:1000) (Pazour *et al.*, 2002), anti-Pericentrin (Abcam, ab4448, 1:1000), anti-Rpgr (gift from Dr. T. Li, 1:1000) (Hong *et al.*, 2003), anti-FLAG (Sigma, F7425, 1:1000), anti-(pThr^{674}) Kif3a (1:250), anti-IFT88 (Proteintech Group, 13967-1-AP, 1:500), and anti-Arl13b (Proteintech Group, 17711-1-AP, 1:500); goat polyclonal anti-MCH1R (Santa Cruz, C-17, 1:500) and anti-SSTR3 (Santa Cruz, M-18, 1:500); guinea pig polyclonal anti-ICK (1:50), anti-Gli2 (gift from Dr. J. T. Eggenschwiler, 1:1000) (Cho *et al.*, 2008), and anti-Mak (1:1000) (Omori *et al.*, 2010) antibodies. Mouse monoclonal antibodies against Islet1/2, HNF3B, HB9, Nkx2.2, Pax6, Pax7, Shh, and Nkx6.1 were obtained from the Developmental Studies Hybridoma Bank. We used Cy3-conjugated secondary antibodies (Jackson ImmunoResearch Laboratories, 1:500), Alexa Fluor 488-conjugated secondary antibodies (Sigma, 1:500), and DyLight 649-cojugated secondary antibodies (Jackson ImmunoResearch Laboratories, 1:500).

Plasmid constructs

A full-length cDNA fragment of mouse ICK was amplified by PCR using the RIKEN full-length enriched library clone (GenBank accession no. AK087484) containing a missense mutation (Leu260Pro) as a template, and cloned into the pCAGGSII expression vector (Omori *et al.*, 2010). This missense mutation was corrected by PCR primers. A full-length cDNA fragment of human ICK was amplified by PCR using a

human ICK clone obtained from PlasmID (GenBank accession no. BC136420) as a template, and cloned into the pCAGGSII vector. The mouse ICK K33R mutation and human ICK R272Q mutation were introduced by PCR primers. Full-length cDNA fragments of mouse IFT57 and BBS8 were amplified by PCR using the RIKEN full-length enriched library clone (IFT57, GenBank accession no. AK047217; BBS8, GenBank accession no. AK081697) as a template, and cloned into the pCAGGSII expression vector. A full-length cDNA fragment of mouse Kif3a was amplified by PCR using a mouse Kif3a clone obtained from Open Biosystems (GenBank accession no. BC052707) as a template, and cloned into the pCAGGSII vector. Full-length cDNA fragments of mouse IFT88 and IFT140 were amplified by PCR using a mouse P0 retinal cDNA library and cloned into the pCAGGSII expression vector. A cDNA fragment encoding a partial sequence of mouse Kif3a (Kif3a-C, residues 455-701) was amplified by PCR using a mouse Kif3a clone obtained from Open Biosystems (GenBank accession no. BC052707) as a template, and cloned into the pGEX4T-1 vector (GE Healthcare). For *Kif3a* knockdown, pBAsi-mU6 was used for DNA vector-based shRNA synthesis. Three target sequences, GGGTGAACTTGGAGAAG ATGG (shKif3a-1), GGACCTTCTGAAAGCCCAACA (shKif3a-2), and GCCTGAGA CCGTAATTGATTC (shKif3a-3), were selected from different positions in the mouse *Kif3a* open reading frame and subcloned into the pBAsi-mU6 vector. To construct plasmids encoding shKif3a-1-resistant Kif3a, seven silent mutations in the target sequence were introduced by PCR-based mutagenesis.

Statistical analysis

Data are presented as means ± SD. Statistical significance was evaluated using a Mann-Whitney test (Figure 7O) or a Student's *t* test (other Figures), and $p < 0.05$ was taken to be statistically significant.

Acknowledgements

We thank Dr. R. Kageyama (Kyoto Universisty) for the Nestin-Cre mouse; Drs. S. J. Scales (Genentech), K. V. Anderson (Sloan-Kettering Institute), G. J. Pazour (University of Massachusetts Medical School), T. Li (National Institutes of Health), and J. T. Eggenschwiler (Princeton University) for reagents; Drs. S. Kondo and M. Watanabe (Osaka University) for help with zebrafish embryos; M. Kadowaki, A. Tani, A. Ishimaru, Y. Saioka, H. Abe, and S. Kennedy for technical assistance. This work was supported by CREST and PRESTO from Japan Science and Technology Agency, a grant for Molecular Brain Science, Grants-in-Aid for Scientific Research on Priority Areas, Grant-in-Aid for Scientific Research (B), Young Scientists (B), Specially Designated Research Promotion and Scientific Research on Innovative Areas from the Ministry of Education, Culture, Sports, Science and Technology of Japan, The Takeda Science Foundation, The Uehara Memorial Foundation, Research Foundation for Opto-Science and Technology, The Mitsubishi Foundation, Suzuken Memorial Foundation, and Japan Foundation for Applied Enzymology. A part of this work was supported by "Nanotechnology Platform" (project No. 12024046) of the Ministry of Education, Culture, Sports, Science and Technology (MEXT), Japan.

Author Contributions

TC, YO, and TF designed the project. TC, YO, and TF performed the molecular and *in situ* hybridization experiments. TF generated the floxed mice. TC and YO carried out immunohistochemical analysis. TC performed cell culture experiments. YO carried out rescue experiments using zebrafish embryos. TC and RK performed scanning electron microscopic analysis. TC, YO, and TF wrote the manuscript. TF supervised the project.

Conflict of Interest

The authors declare that they have no conflict of interest.

Supplementary data

Supplementary data are available at *The EMBO Journal* Online.

References

Altman J, Bayer SA (1990) Migration and distribution of two populations of hippocampal granule cell precursors during the perinatal and postnatal periods. *J Comp Neurol* **301**:365-381

Arellano JI, Guadiana SM, Breunig JJ, Rakic P, Sarkisian MR (2012) Development and distribution of neuronal cilia in mouse neocortex. *J Comp Neurol* **520**:848-873

Asleson CM, Lefebvre PA (1998) Genetic analysis of flagellar length control in Chlamydomonas reinhardtii: a new long-flagella locus and extragenic suppressor mutations. *Genetics* **148**:693-702

Bengs F, Scholz A, Kuhn D, Wiese M (2005) LmxMPK9, a mitogen-activated protein kinase homologue affects flagellar length in Leishmania mexicana. *Mol Microbiol* **55**:1606-1615

Berbari NF, Lewis JS, Bishop GA, Askwith CC, Mykytyn K (2008) Bardet-Biedl syndrome proteins are required for the localization of G protein-coupled receptors to primary cilia. *Proc Natl Acad Sci U S A* **105**:4242-4246

Berman SA, Wilson NF, Haas NA, Lefebvre PA (2003) A novel MAP kinase regulates flagellar length in Chlamydomonas. *Curr Biol* **13**:1145-1149

Besse L, Neti M, Anselme I, Gerhardt C, Ruther U, Laclef C, Schneider-Maunoury S (2011) Primary cilia control telencephalic patterning and morphogenesis via Gli3 proteolytic processing. *Development* **138**:2079-2088

Bishop GA, Berbari NF, Lewis J, Mykytyn K (2007) Type III adenylyl cyclase localizes to primary cilia throughout the adult mouse brain. *J Comp Neurol* **505**:562-571

Breunig JJ, Sarkisian MR, Arellano JI, Morozov YM, Ayoub AE, Sojitra S, Wang B, Flavell RA, Rakic P, Town T (2008) Primary cilia regulate hippocampal neurogenesis by mediating sonic hedgehog signaling. *Proc Natl Acad Sci U S A* **105**:13127-13132

Burghoorn J, Dekkers MP, Rademakers S, de Jong T, Willemsen R, Jansen G (2007) Mutation of the MAP kinase DYF-5 affects docking and undocking of kinesin-2 motors and reduces their speed in the cilia of Caenorhabditis elegans. *Proc Natl Acad Sci U S A* **104**:7157-7162

Carter CS, Vogel TW, Zhang Q, Seo S, Swiderski RE, Moninger TO, Cassell MD, Thedens DR, Keppler-Noreuil KM, Nopoulos P, Nishimura DY, Searby CC, Bugge K, Sheffield VC (2012) Abnormal development of NG2+PDGFR-alpha+ neural progenitor cells leads to neonatal hydrocephalus in a ciliopathy mouse model. *Nat Med* **18**:1797-1804

Chizhikov VV, Davenport J, Zhang Q, Shih EK, Cabello OA, Fuchs JL, Yoder BK,

Millen KJ (2007) Cilia proteins control cerebellar morphogenesis by promoting expansion of the granule progenitor pool. *J Neurosci* **27**:9780-9789

Cho A, Ko HW, Eggenschwiler JT (2008) FKBP8 cell-autonomously controls neural tube patterning through a Gli2- and Kif3a-dependent mechanism. *Dev Biol* **321**:27-39

Corbit KC, Aanstad P, Singla V, Norman AR, Stainier DY, Reiter JF (2005) Vertebrate Smoothened functions at the primary cilium. *Nature* **437**:1018-1021

Czarnecki PG, Shah JV (2012) The ciliary transition zone: from morphology and molecules to medicine. *Trends Cell Biol* **22**:201-210

Davenport JR, Watts AJ, Roper VC, Croyle MJ, van Groen T, Wyss JM, Nagy TR, Kesterson RA, Yoder BK (2007) Disruption of intraflagellar transport in adult mice leads to obesity and slow-onset cystic kidney disease. *Curr Biol* **17**:1586-1594

Dehay C, Kennedy H (2007) Cell-cycle control and cortical development. *Nat Rev Neurosci* **8**:438-450

Deng C, Wynshaw-Boris A, Zhou F, Kuo A, Leder P (1996) Fibroblast growth factor receptor 3 is a negative regulator of bone growth. *Cell* **84**:911-921

Dessaud E, McMahon AP, Briscoe J (2008) Pattern formation in the vertebrate neural tube: a sonic hedgehog morphogen-regulated transcriptional network. *Development* **135**:2489-2503

Fliegauf M, Benzing T, Omran H (2007) When cilia go bad: cilia defects and ciliopathies. *Nat Rev Mol Cell Biol* **8**:880-893

Fu Z, Schroeder MJ, Shabanowitz J, Kaldis P, Togawa K, Rustgi AK, Hunt DF, Sturgill TW (2005) Activation of a nuclear Cdc2-related kinase within a mitogen-activated protein kinase-like TDY motif by autophosphorylation and cyclin-dependent protein kinase-activating kinase. *Mol Cell Biol* **25**:6047-6064

Fu Z, Larson KA, Chitta RK, Parker SA, Turk BE, Lawrence MW, Kaldis P, Galaktionov K, Cohn SM, Shabanowitz J, Hunt DF, Sturgill TW (2006) Identification of yin-yang regulators and a phosphorylation consensus for male germ cell-associated kinase (MAK)-related kinase. *Mol Cell Biol* **26**:8639-8654

Gerdes JM, Davis EE, Katsanis N (2009) The vertebrate primary cilium in development, homeostasis, and disease. *Cell* **137**:32-45

Han YG, Spassky N, Romaguera-Ros M, Garcia-Verdugo JM, Aguilar A, Schneider-Maunoury S, Alvarez-Buylla A (2008) Hedgehog signaling and primary cilia are required for the formation of adult neural stem cells. *Nat Neurosci* **11**:277-284

Handel M, Schulz S, Stanarius A, Schreff M, Erdtmann-Vourliotis M, Schmidt H, Wolf G, Hollt V (1999) Selective targeting of somatostatin receptor 3 to neuronal cilia. *Neuroscience* **89**:909-926

Haycraft CJ, Banizs B, Aydin-Son Y, Zhang Q, Michaud EJ, Yoder BK (2005) Gli2 and Gli3 localize to cilia and require the intraflagellar transport protein polaris for processing and function. *PLoS Genet* **1**:e53

Hong DH, Pawlyk B, Sokolov M, Strissel KJ, Yang J, Tulloch B, Wright AF, Arshavsky VY, Li T (2003) RPGR isoforms in photoreceptor connecting cilia and the transitional zone of motile cilia. *Invest Ophthalmol Vis Sci* **44**:2413-2421

Huangfu D, Anderson KV (2005) Cilia and Hedgehog responsiveness in the mouse. *Proc Natl Acad Sci U S A* **102**:11325-11330

Isaka F, Ishibashi M, Taki W, Hashimoto N, Nakanishi S, Kageyama R (1999) Ectopic expression of the bHLH gene Math1 disturbs neural development. *Eur J Neurosci* **11**:2582-2588

Ishikawa H, Marshall WF (2011) Ciliogenesis: building the cell's antenna. *Nat Rev Mol Cell Biol* **12**:222-234

Kim J, Kato M, Beachy PA (2009) Gli2 trafficking links Hedgehog-dependent activation of Smoothened in the primary cilium to transcriptional activation in the nucleus. *Proc Natl Acad Sci U S A* **106**:21666-21671

Ko HW, Norman RX, Tran J, Fuller KP, Fukuda M, Eggenschwiler JT (2010) Broad-minded links cell cycle-related kinase to cilia assembly and hedgehog signal transduction. *Dev Cell* **18**:237-247

Lahiry P, Wang J, Robinson JF, Turowec JP, Litchfield DW, Lanktree MB, Gloor GB, Puffenberger EG, Strauss KA, Martens MB, Ramsay DA, Rupar CA, Siu V, Hegele RA (2009) A multiplex human syndrome implicates a key role for intestinal cell kinase in development of central nervous, skeletal, and endocrine systems. *Am J Hum Genet* **84**:134-147

Li G, Pleasure SJ (2005) Morphogenesis of the dentate gyrus: what we are learning from mouse mutants. *Dev Neurosci* **27**:93-99

Louvi A, Grove EA (2011) Cilia in the CNS: the quiet organelle claims center stage. *Neuron* **69**:1046-1060

Marley A, von Zastrow M (2010) DISC1 regulates primary cilia that display specific dopamine receptors. *PLoS One* **5**:e10902

Muranishi Y, Terada K, Inoue T, Katoh K, Tsujii T, Sanuki R, Kurokawa D, Aizawa S, Tamaki Y, Furukawa T (2011) An essential role for RAX homeoprotein and NOTCH-HES signaling in Otx2 expression in embryonic retinal photoreceptor

cell fate determination. *J Neurosci* **31**:16792-16807

Nigg EA, Raff JW (2009) Centrioles, centrosomes, and cilia in health and disease. *Cell* **139**:663-678

Ocbina PJ, Eggenschwiler JT, Moskowitz I, Anderson KV (2011) Complex interactions between genes controlling trafficking in primary cilia. *Nat Genet* **43**:547-553

Omori Y, Zhao C, Saras A, Mukhopadhyay S, Kim W, Furukawa T, Sengupta P, Veraksa A, Malicki J (2008) Elipsa is an early determinant of ciliogenesis that links the IFT particle to membrane-associated small GTPase Rab8. *Nat Cell Biol* **10**:437-444

Omori Y, Chaya T, Katoh K, Kajimura N, Sato S, Muraoka K, Ueno S, Koyasu T, Kondo M, Furukawa T (2010) Negative regulation of ciliary length by ciliary male germ cell-associated kinase (Mak) is required for retinal photoreceptor survival. *Proc Natl Acad Sci U S A* **107**:22671-22676

Pazour GJ, Baker SA, Deane JA, Cole DG, Dickert BL, Rosenbaum JL, Witman GB, Besharse JC (2002) The intraflagellar transport protein, IFT88, is essential for vertebrate photoreceptor assembly and maintenance. *J Cell Biol* **157**:103-113

Pedersen LB, Geimer S, Rosenbaum JL (2006) Dissecting the molecular mechanisms of intraflagellar transport in chlamydomonas. *Curr Biol* **16**:450-459

Pedersen LB, Miller MS, Geimer S, Leitch JM, Rosenbaum JL, Cole DG (2005) Chlamydomonas IFT172 is encoded by FLA11, interacts with CrEB1, and regulates IFT at the flagellar tip. *Curr Biol* **15**:262-266

Phirke P, Efimenko E, Mohan S, Burghoorn J, Crona F, Bakhoum MW, Trieb M, Schuske K, Jorgensen EM, Piasecki BP, Leroux MR, Swoboda P (2011) Transcriptional profiling of C. elegans DAF-19 uncovers a ciliary base-associated protein and a CDK/CCRK/LF2p-related kinase required for intraflagellar transport. *Dev Biol* **357**:235-247

Qin J, Lin Y, Norman RX, Ko HW, Eggenschwiler JT (2011) Intraflagellar transport protein 122 antagonizes Sonic Hedgehog signaling and controls ciliary localization of pathway components. *Proc Natl Acad Sci U S A* **108**:1456-1461

Rosenbaum JL, Witman GB (2002) Intraflagellar transport. *Nat Rev Mol Cell Biol* **3**:813-825

Sakagami K, Gan L, Yang XJ (2009) Distinct effects of Hedgehog signaling on neuronal fate specification and cell cycle progression in the embryonic mouse retina. *J Neurosci* **29**:6932-6944

Sakai K, Miyazaki J (1997) A transgenic mouse line that retains Cre recombinase activity in mature oocytes irrespective of the cre transgene transmission.

Biochem Biophys Res Commun **237**:318-324

Sato S, Inoue T, Terada K, Matsuo I, Aizawa S, Tano Y, Fujikado T, Furukawa T (2007) Dkk3-Cre BAC transgenic mouse line: a tool for highly efficient gene deletion in retinal progenitor cells. *Genesis* **45**:502-507

Sotelo C (2004) Cellular and genetic regulation of the development of the cerebellar system. *Prog Neurobiol* **72**:295-339

Spassky N, Merkle FT, Flames N, Tramontin AD, Garcia-Verdugo JM, Alvarez-Buylla A (2005) Adult ependymal cells are postmitotic and are derived from radial glial cells during embryogenesis. *J Neurosci* **25**:10-18

Spassky N, Han YG, Aguilar A, Strehl L, Besse L, Laclef C, Ros MR, Garcia-Verdugo JM, Alvarez-Buylla A (2008) Primary cilia are required for cerebellar development and Shh-dependent expansion of progenitor pool. *Dev Biol* **317**:246-259

Tissir F, Qu Y, Montcouquiol M, Zhou L, Komatsu K, Shi D, Fujimori T, Labeau J, Tyteca D, Courtoy P, Poumay Y, Uemura T, Goffinet AM (2010) Lack of cadherins Celsr2 and Celsr3 impairs ependymal ciliogenesis, leading to fatal hydrocephalus. *Nat Neurosci* **13**:700-707

Togawa K, Yan YX, Inomoto T, Slaugenhaupt S, Rustgi AK (2000) Intestinal cell kinase (ICK) localizes to the crypt region and requires a dual phosphorylation site found in map kinases. *J Cell Physiol* **183**:129-139

Tsao CC, Gorovsky MA (2008) Different effects of Tetrahymena IFT172 domains on anterograde and retrograde intraflagellar transport. *Mol Biol Cell* **19**:1450-1461

Tsujikawa M, Malicki J (2004) Intraflagellar transport genes are essential for differentiation and survival of vertebrate sensory neurons. *Neuron* **42**:703-716

Wang Y, Dakubo GD, Thurig S, Mazerolle CJ, Wallace VA (2005) Retinal ganglion cell-derived sonic hedgehog locally controls proliferation and the timing of RGC development in the embryonic mouse retina. *Development* **132**:5103-5113

Wei Q, Zhang Y, Li Y, Zhang Q, Ling K, Hu J (2012) The BBSome controls IFT assembly and turnaround in cilia. *Nat Cell Biol* **14**:950-957

Wen X, Lai CK, Evangelista M, Hongo JA, de Sauvage FJ, Scales SJ (2010) Kinetics of hedgehog-dependent full-length Gli3 accumulation in primary cilia and subsequent degradation. *Mol Cell Biol* **30**:1910-1922

Willaredt MA, Hasenpusch-Theil K, Gardner HA, Kitanovic I, Hirschfeld-Warneken VC, Gojak CP, Gorgas K, Bradford CL, Spatz J, Wolfl S, Theil T, Tucker KL (2008) A crucial role for primary cilia in cortical morphogenesis. *J Neurosci* **28**:12887-12900

Xia L, Robinson D, Ma AH, Chen HC, Wu F, Qiu Y, Kung HJ (2002) Identification of human male germ cell-associated kinase, a kinase transcriptionally activated by androgen in prostate cancer cells. *J Biol Chem* **277**:35422-35433

Yang Y, Roine N, Makela TP (2013) CCRK depletion inhibits glioblastoma cell proliferation in a cilium-dependent manner. *EMBO Rep* **14**:741-747

Figure legends

Figure 1 Loss of *ICK* causes defects in development and ciliogenesis. (**A**) Image of $ICK^{+/+}$ (center), $ICK^{+/-}$ (left), and $ICK^{-/-}$ (right) embryos at E17.5. (**B–E**) Skeletal defects in $ICK^{-/-}$ limbs and digits. (**B–D**) Alizarin Red and Alcian Blue staining of forelimbs from $ICK^{+/+}$ and $ICK^{-/-}$ mice at E18.5. (**B, C**) Forelimbs exhibited pre-axial polydactyly in $ICK^{-/-}$ embryos. (**D, E**) The distal long bone length of both forelimb and posterior limb was shorter in $ICK^{-/-}$ mice compared with that in $ICK^{+/+}$ mice. (**F, G**) Nissl-stained coronal sections from $ICK^{+/+}$ and $ICK^{-/-}$ mice at E17.5. $ICK^{-/-}$ mice showed hydrocephalus (**G**). (**H–I'**) The cilia in the cerebral cortex of $ICK^{+/+}$ (**H, H'**) and $ICK^{-/-}$ (**I, I'**) mice at E15.5 were stained with an anti-Adenylate Cyclase 3 (AC3) antibody (green). Ciliary numbers on the neuroepithelial cells (arrowheads) in the cerebral cortex are reduced in $ICK^{-/-}$ mice. (**J, K**) Scanning electron microscopic analysis of $ICK^{+/+}$ (**J**) and $ICK^{-/-}$ (**K**) neural tube cilia at E10.5. Cilia are shorter in the $ICK^{-/-}$ neural tube. (**L, M**) ICK is localized at cilia tips. $ICK^{+/+}$ and $ICK^{-/-}$ MEFs were immunostained with antibodies against ICK (red), acetylated α-tubulin (a marker for the ciliary axoneme, green), and Pericentrin (a marker for centrosomes, magenta). Arrowheads indicate ciliary tips. (**N–Q**) Ciliary defects in $ICK^{-/-}$ MEFs. $ICK^{+/+}$ and $ICK^{-/-}$ MEFs were immunostained with antibodies against Pericentrin and acetylated α-tubulin (green). The numbers (**P**) and length (**Q**) of the cilia stained with an antibody against acetylated α-tubulin were measured. The cilia in $ICK^{-/-}$ MEFs are markedly fewer and shorter. Nuclei were stained with DAPI (blue). Scale bars, 10 mm (**A**), 2 mm (**B–D**), 1 mm (**F, G**), 100 μm (**H, I**), 20 μm (left panels in **N, O**), 10 μm (**H', I'**, left panels in **L, M**), 2 μm (right panels in **N, O**), 1 μm (center and right panels in **L, M**),

and 500 nm (**J, K**). Error bars show the SD. *$p < 0.03$.

Figure 2 Loss of *ICK* affects retinal and cerebellar development. (**A–C**) The cilia in retinal neuroepithelial cells from the P0 control and *ICK Dkk3* CKO mice were immunostained with an antibody against AC3 (green in **A, B**). The number of AC3-positive cilia in P0 control and *ICK Dkk3* CKO retinas were counted (**C**). Ciliary numbers were reduced in the *ICK Dkk3* CKO retina. (**D**) Dorsal view of the dissected brain from control and *ICK Nes* CKO mice at the age of one month. The cerebellum (arrowheads) is smaller in *ICK Nes* CKO mice (right) compared to that in control mice (left). (**E–H**) Nissl staining of cerebellar (**E, F**) and hippocampal (**G, H**) sections from P21 control (**E, G**) and *ICK Nes* CKO (**F, H**) mice. The lobes of the cerebellum are markedly smaller in *ICK Nes* CKO mice (**F**) compared to those in control mice (**E**). The hippocampal DG is smaller in *ICK Nes* CKO mice (**H**) compared to that in control mice (**G**). (**I–L**) Immunohistochemical analysis of the *ICK Nes* CKO cerebellum with cell proliferation markers. Sagittal cerebellar sections were immunostained with antibodies against Ki67 (green in **I, J**) and PH3 (green in **K, L**). The external granule cell layer (EGL, shown with arrowheads) is thinner in *ICK Nes* CKO mice. (**M–O**) The cilia in EGL cells of the control (**M**) and *ICK Nes* CKO (**N**) mice were stained with an antibody against AC3. The cilia in the EGL are fewer in the *ICK Nes* CKO cerebellum. The number of AC3-positive cilia in the control and *ICK Nes* CKO EGL was counted (**O**). Nuclei were stained with DAPI (blue). Scale bars, 5 mm (**D**), 1 mm (**E, F**), 500 μm (**G, H**), 100 μm (**I–L**), and 5 μm (**A, B, M, N**). Error bars show the SD. *$p < 0.03$. NBL, neuroblastic layer.

Figure 3 ICK is required for ciliogenesis in the developing hippocampal DG. (**A–B'**) Sagittal hippocampal sections from P4 control and *ICK Nes* CKO mice were immunostained with antibodies against Ki67 (red) and AC3 (green). Numbers of Ki67-positive cells with the cilia were decreased in the *ICK Nes* CKO DG. Arrowheads indicate cilia on Ki67-positive cells. (**C**) The percentage of Ki67-positive cells with AC3-positive cilia was quantified. (**D–G'**) Immunohistochemical analysis of the hippocampal DG (**D–E'**) and cerebral cortex (**F–G'**) from one month-old control (**D, D', F, F'**) and *ICK Nes* CKO (**E, E', G, G'**) mice. Coronal sections were stained with antibodies against NeuN (a neuronal marker, red) and AC3 (green). No obvious difference in ciliary number or ciliary length was observed between control and *ICK Nes* CKO mice. (**H, I**) The numbers (**H**) and length (**I**) of the cilia stained with an anti-AC3 antibody were measured. There was no significant difference between the control and *ICK Nes* CKO cerebral cortex. (**J–K'**) Ciliary localization of GPCR in the *ICK Nes* CKO cerebral cortex. Sections from cerebral cortex were stained with ciliary GPCR, MCH1R (red). The cilia were stained with an anti-AC3 antibody (green). MCH1R (arrowheads) was localized in the cilia properly both in control and *ICK Nes* CKO mice. Nuclei were stained with DAPI (blue). Scale bars, 20 μm (**D, E, F, G**) and 10 μm (**A–B', D', E', F', G', J–K'**). Error bars show the SD. **p* < 0.03. n.s., not significant.

Figure 4 Signal-dependent ciliary transport of Shh components is defective in $ICK^{-/-}$ cells. (**A–H**) $ICK^{+/+}$ and $ICK^{-/-}$ MEFs were treated or not treated with Smo agonist (SAG) and immunostained with antibodies against Smo (green in **A–D**) and Gli3 (green in **E–H**). The cilia were immunostained with antibodies against acetylated α-tubulin

(red in **A–D**) or AC3 (red in **E–H**). Smo and Gli3 are aberrantly present in the *ICK*$^{-/-}$ MEF cilia without stimulation with SAG. (**I, J**) Quantification of the cilia with Smo and Gli3 signals. The percentages of the cilia with Smo (**I**) and Gli3 (**J**) signals in *ICK*$^{+/+}$ and *ICK*$^{-/-}$ MEFs with or without treatment of SAG were quantified. (**K, L**) *ICK*$^{+/+}$ (**K**) and *ICK*$^{-/-}$ (**L**) neural tube cilia were immunostained with antibodies against Smo (red) and polyglutamylated tubulin (green). Arrowheads indicate Smo-positive cilia. Smo signals increased in *ICK*$^{-/-}$ neural tube cilia at E10.5. (**M, N**) Cilia in paraxial mesoderm regions of E10.5 *ICK*$^{+/+}$ (**M**) and *ICK*$^{-/-}$ (**N**) embryos were immunostained with antibodies against Smo (red) and polyglutamylated tubulin (green). Smo signals in the cilia increased in *ICK*$^{-/-}$ mice. Nuclei were stained with DAPI (blue). Scale bars, 2 μm (**A–H**) and 1 μm (**K–N**). Error bars show the SD. *$p < 0.03$.

Figure 5 A kinase-dead mutant and an ECO-associated mutant of ICK show a decreased ability to rescue shortened cilia phenotype in *ICK*$^{-/-}$ MEFs. (**A–F**) Kinase activity of ICK is required for ciliary formation but not for localization in the cilia. (**A**) Schematic representation of a kinase-dead ICK. (**B–D**) Constructs expressing FLAG-tagged GFP (**B**), wild-type ICK (ICK-WT; **C**), or kinase-dead ICK K33R (ICK-KD; **D**) were transfected into *ICK*$^{-/-}$ MEFs. Localization of FLAG-tagged proteins was observed using anti-FLAG (green) and anti-acetylated α-tubulin (red) antibodies. (**E**) The number of cilia stained with an anti-acetylated α-tubulin antibody was counted. (**F**) The length of cilia stained with anti-acetylated α-tubulin antibody was measured. (**G–O**) The ECO-associated mutant of human ICK has a decreased ability to induce ciliary formation. (**G**) Schematic representation of the ECO-associated mutant of human ICK. (**H–J**) FLAG-tagged constructs expressing GFP (**H**), wild-type human ICK

(hICK-WT; **I**), or ECO-associated mutant R272Q of human ICK (hICK-ECO; **J**) were transfected into NIH3T3 cells. Localization of FLAG-tagged proteins was observed using anti-FLAG (green) and anti-acetylated α-tubulin (red) antibodies. (**K**) The percentage of the cilia with the FLAG signal was quantified. (**L–N**) The FLAG-tagged GFP- (**L**), hICK-WT- (**M**), or hICK-ECO- (**N**) expressing plasmid was transfected into *ICK*$^{-/-}$ MEFs. (**O**) The number of cilia stained with anti-acetylated α-tubulin antibody was counted. Nuclei were stained with DAPI (blue). Scale bars, 5 μm (**B–D, L–N**) and 2 μm (**H–J**). Error bars show the SD. *$p < 0.03$. Arrowheads indicate ciliary tips.

Figure 6 Loss or overexpression of ICK affects ciliary localization of IFT components. (**A–G**) IFT components concentrated at cilia tips in *ICK*$^{-/-}$ MEFs. (**A–D**) *ICK*$^{+/+}$ and *ICK*$^{-/-}$ MEFs were stained with anti-IFT88 (**A, B**) and anti-IFT144 (**C, D**) antibodies. (**E**) The number of cilia with a concentration of IFT88 at ciliary tips was measured. (**F, G**) FLAG-tagged BBS8-expressing plasmid was transfected into *ICK*$^{+/+}$ and *ICK*$^{-/-}$ MEFs. Cells were stained with anti-acetylated α-tubulin (red) and anti-FLAG (green) antibodies. (**H–Q**) FLAG-tagged constructs expressing GFP (**H, I**), Kif3a (**J, K**), IFT88 (**L, M, P, Q**), or IFT57 (**N, O**) were transfected with or without an ICK expression plasmid into NIH3T3 cells. Localization of FLAG-tagged proteins was observed using anti-FLAG (green) and anti-acetylated α-tubulin (red) antibodies. (**R**) The number of cilia with the FLAG-tagged protein predominantly localized at ciliary tips was counted. (**S–V**) FLAG-tagged constructs expressing IFT140 (**S, T**) or BBS8 (**U, V**) were transfected with or without an ICK expression plasmid into NIH3T3 cells. Localization of FLAG-tagged proteins was observed using anti-FLAG (green) and anti-acetylated α-tubulin (red) antibodies. Nuclei were stained with DAPI (blue). Scale bars, 2 μm

(**A–D, F–O, S–V**) and 1 μm (**P, Q**). Error bars show the SD. *$p < 0.03$. Arrowheads indicate ciliary tips.

Figure 7 The C-terminal portion of Kif3a is phosphorylated by ICK and Kif3a phosphorylation is essential for proper ciliary formation. (**A**) Schematic representation of mouse full-length Kif3a. (**B**) Amino acid sequence alignment of human KIF3A, mouse Kif3a, zebrafish Kif3a, *C. elegans* Klp-20, and *Chlamydomonas* FLA10 proteins. The predicted amino acid sequences of these proteins were aligned by the ClustalW program (http://clustalw.ddbj.nig.ac.jp/). Asterisks, identical amino acids; colons and periods, similar amino acids. Predicted ICK phosphorylation sites are shown in red. (**C**) ICK phosphorylates Kif3a *in vitro*. GST-tagged C-terminal fragments (residues 455-701) of wild-type Kif3a (GST-Kif3a-C-WT) or T674A Kif3a (GST-Kif3a-C-T674A) were purified from bacterial extracts and stained with Coomassie brilliant blue (left panel). GST-Kif3a deletion proteins were applied to the *in vitro* kinase assay using purified GST-ICK (right panel). (**D, E**) Ciliary localization of p-Kif3a in $ICK^{+/+}$ (**D**) and $ICK^{-/-}$ (**E**) MEFs. Cells were immunostained with antibodies against p-Kif3a (green) and acetylated α-tubulin (red). The proportion of cilia with p-Kif3a signals at ciliary tips decreased in $ICK^{-/-}$ MEFs. Arrowheads indicate ciliary tips. (**F**) The percentage of cilia with p-Kif3a signals at the ciliary tips was quantified. (**G**) The C-terminal amino acid sequence of mouse Kif3a containing eight serine or threonine residues. (**H–M**) FLAG-tagged constructs expressing GFP or shRNA-resistant Kif3a (WT, T674A, or 8xA) were transfected with control shRNA or shKif3a-1 into NIH3T3 cells. Cells were immunostained with anti-FLAG (green) and anti-acetylated α-tubulin (red) antibodies (**H–L**). The number of cilia stained with an anti-acetylated

α-tubulin antibody was counted (**M**). (**N**) Injection with *Kif3a* antisense morpholino (Kif3a MO) into zebrafish embryos causes curly tail, a phenotype characteristic of ciliary defects. (**O**) Quantification of curly tail phenotype larvae injected with wild-type and mutant *Kif3a* mRNA and Kif3a MO. Curly tail phenotype is partially rescued by injection with Kif3a-WT mRNA. The numbers of larvae showing curly tail increased with injection Kif3a-8xA mRNA compared to injection with Kif3a-WT mRNA. (**P–T**) Cilia in nasal pit at 3 dpf larvae were observed by staining of acetylated α-tubulin (red). Representative images of nasal pit from each group were shown. Actin was stained by phalloidin (green). Kif3a-WT mRNA injection partially rescued loss of cilia caused by injection of Kif3a MO, whereas, Kif3a-8xA mRNA injection failed to rescue that. Signal intensity of acetylated α-tubulin staining of cilia in nasal pit was measured (**T**). Nuclei were stained with DAPI (blue). Scale bars, 20 μm (**P–S**), 5 μm (**H–L**), and 2 μm (**D, E**). Error bars show the SD. $*p < 0.03$.

Figure 8 A hypothetical model for ICK function in the regulation of IFT turnaround at ciliary tips. Loss of function of ICK causes the accumulation of components of IFT-A, IFT-B, and BBSome at ciliary tips. Functional defects of cilia observed in *ICK*-deficient cells were probably due to insufficient turnaround of IFT complexes in cilia. Under ICK overexpression conditions, an excess amount of ICK does not affect ciliogenesis but does cause IFT-B (but not IFT-A) subcomplex accumulation at ciliary tips. Accumulation of IFT-B components occasionally forms ring-like structures at cilia tips. ICK may regulate the disassembly between IFT-A and IFT-B subcomplexes at ciliary tips through phosphorylation of Kif3a C-terminal residues.

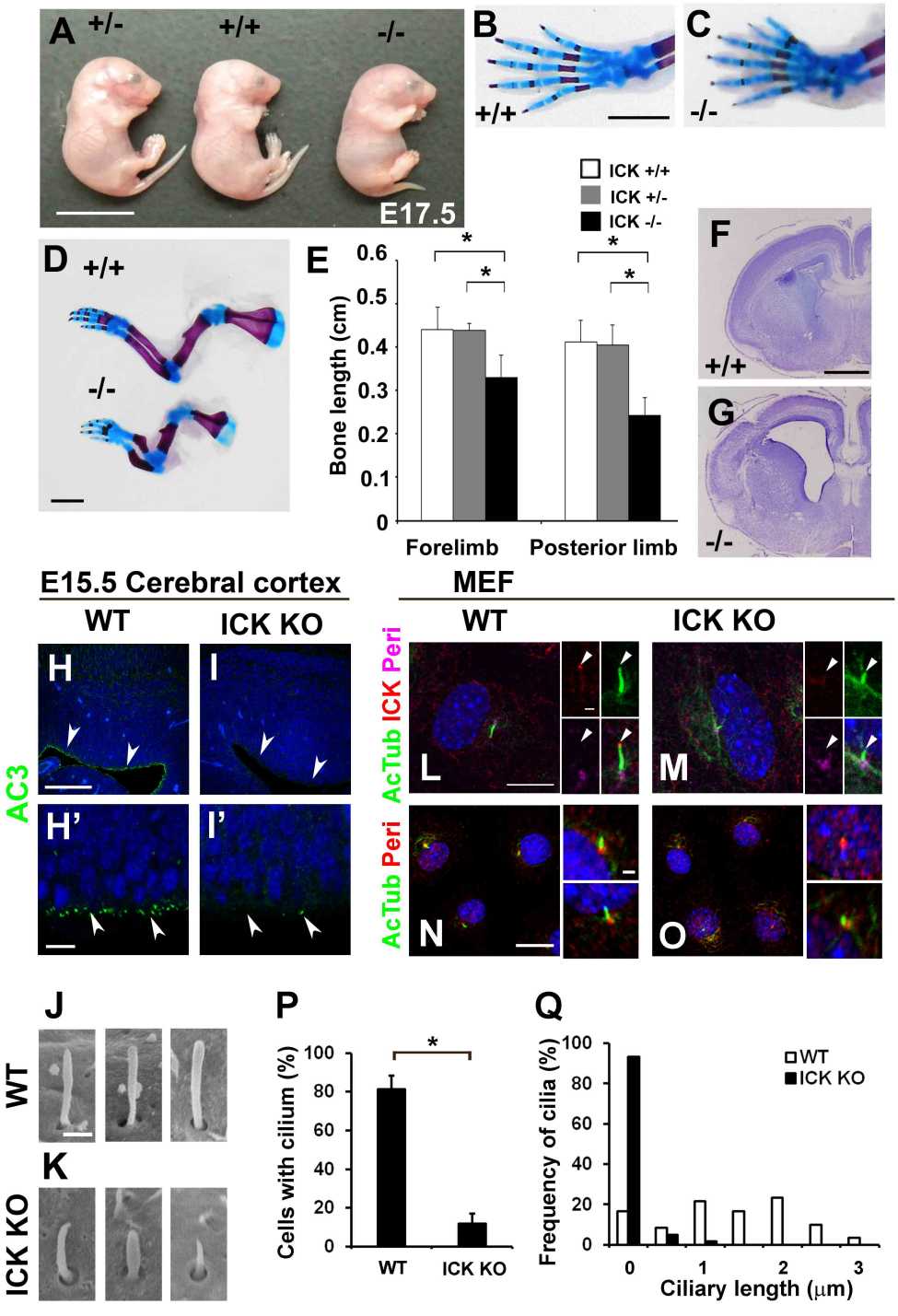

Chaya *et al.*, Figure 1

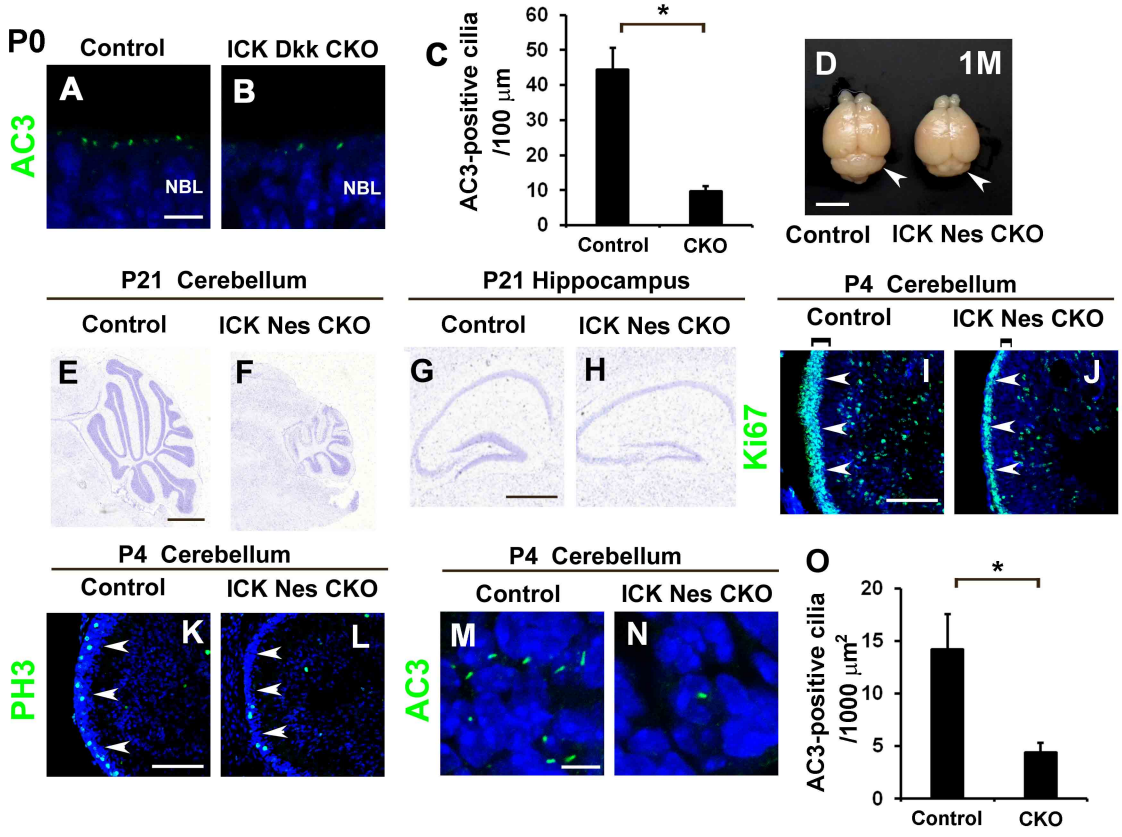

Chaya *et al.*, Figure 2

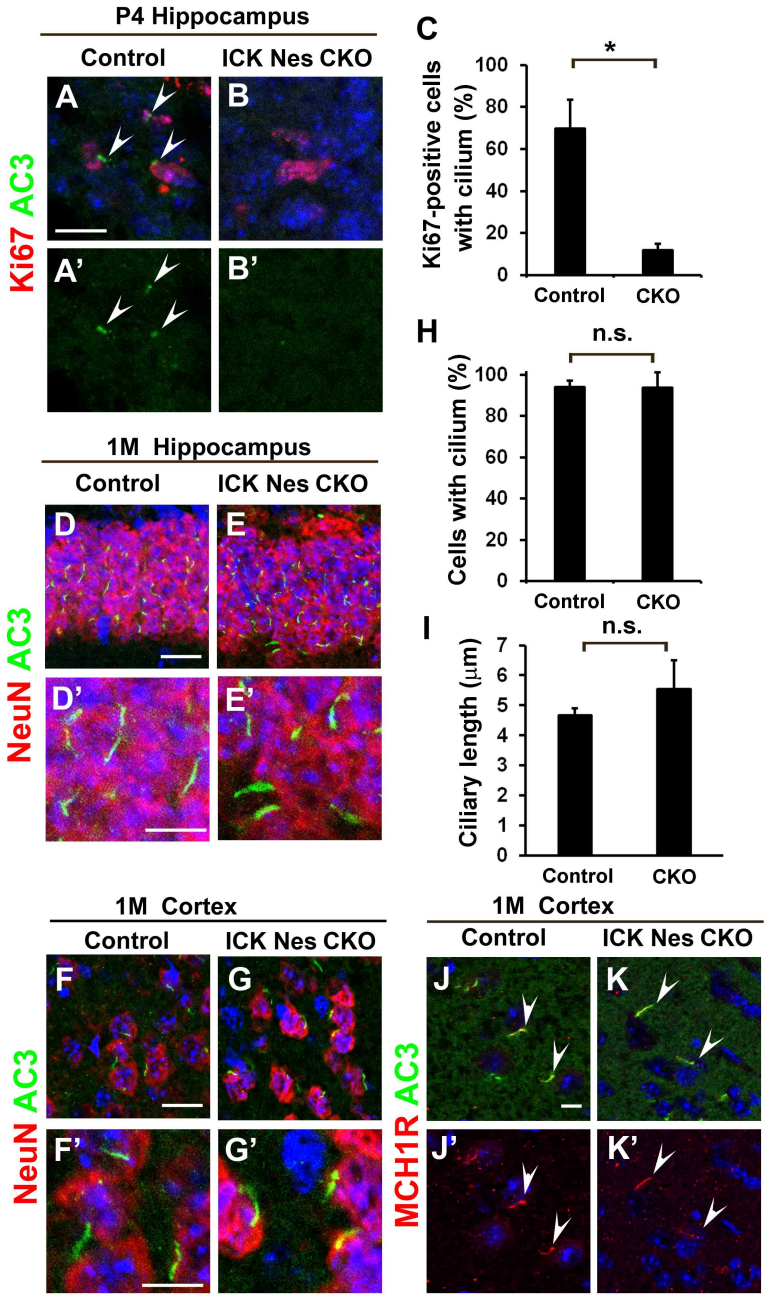

Chaya *et al.*, Figure 3

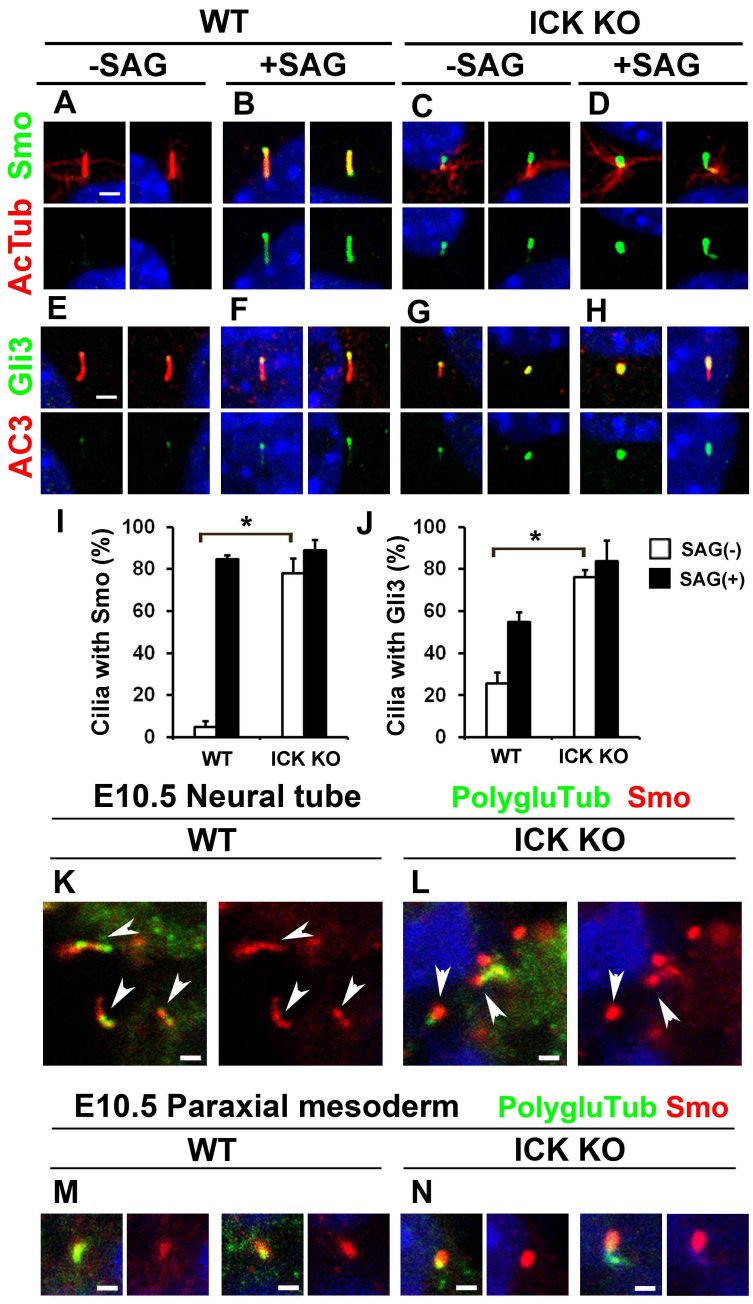

Chaya *et al.*, Figure 4

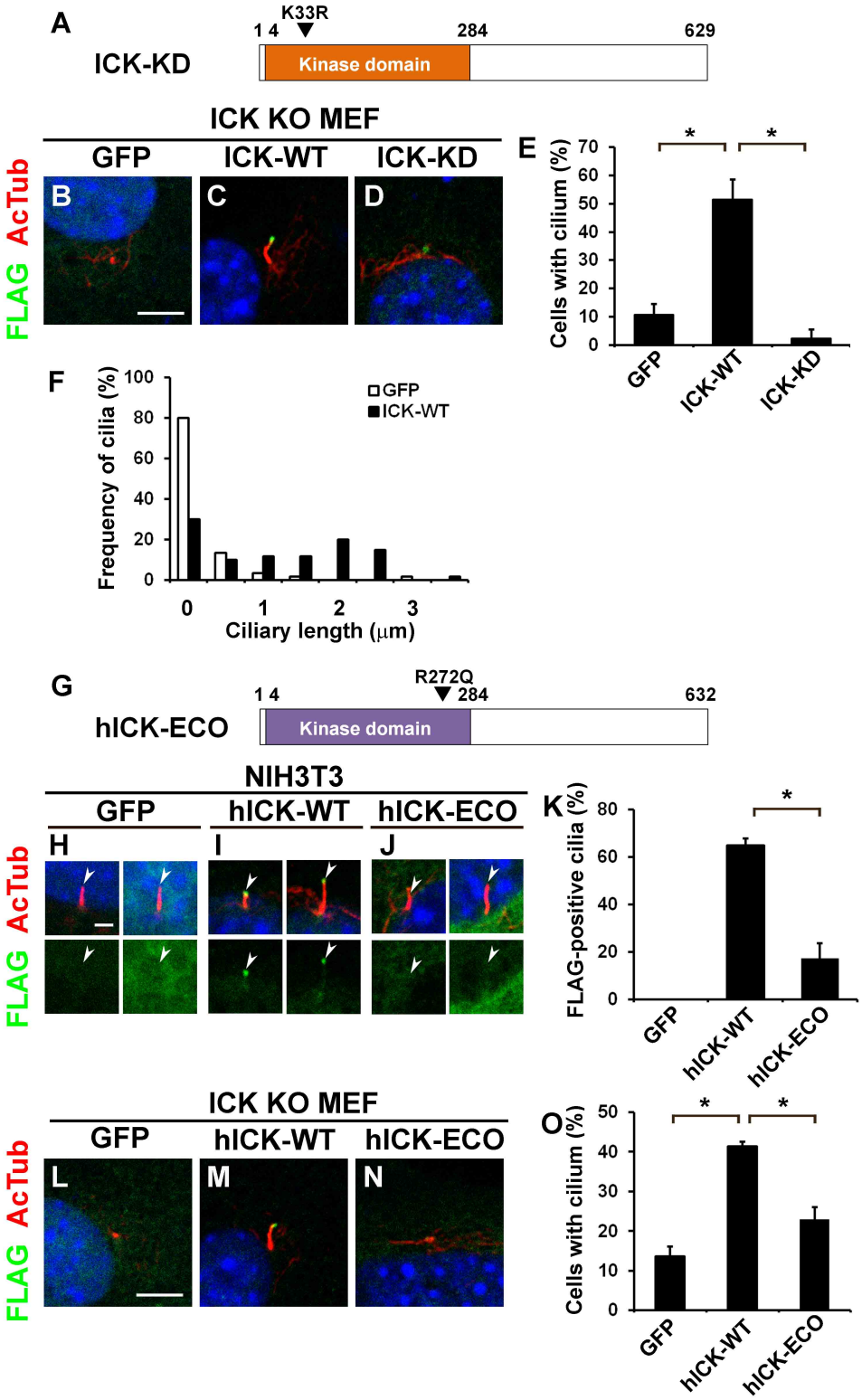

Chaya *et al.*, Figure 5

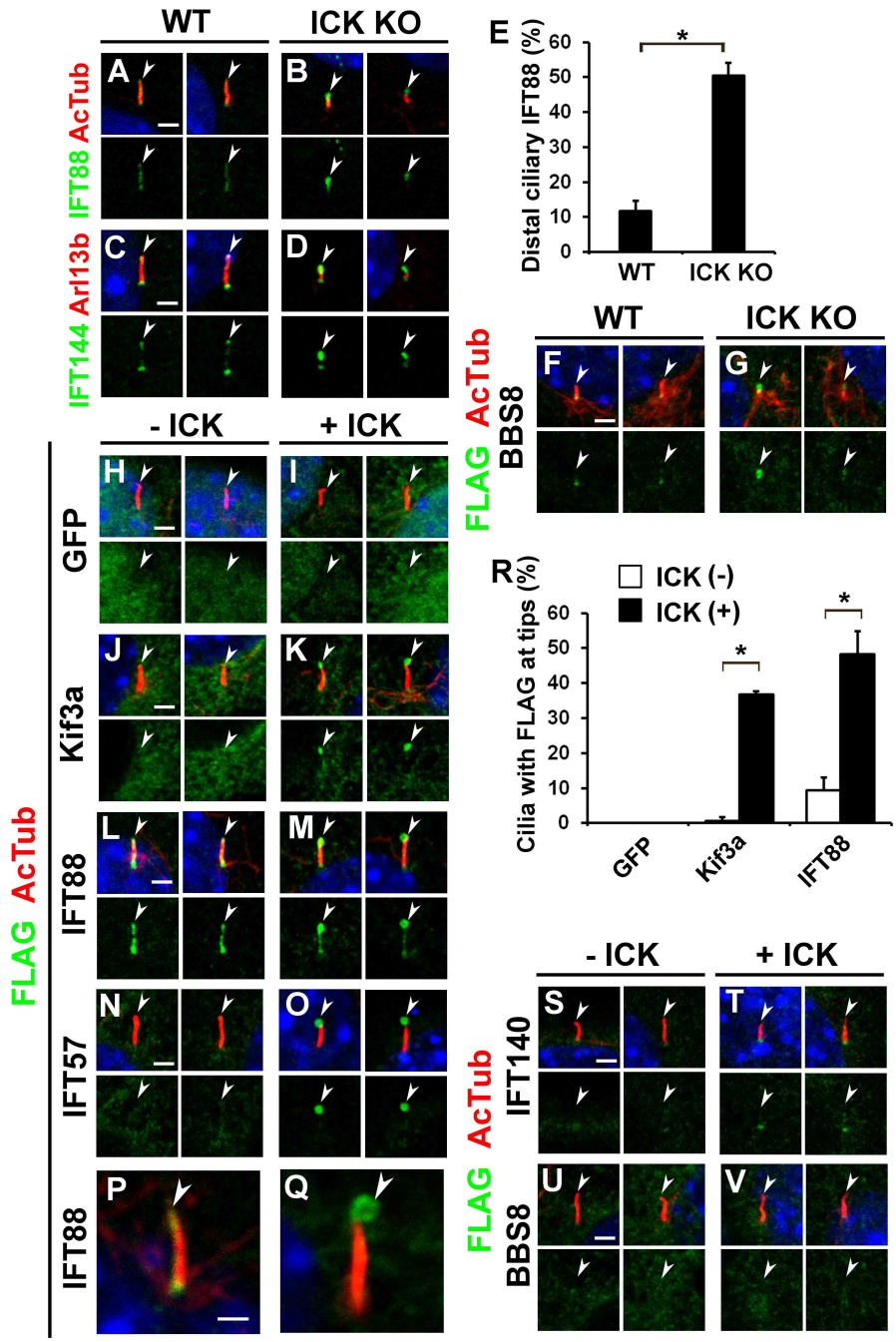

Chaya *et al.*, Figure 6

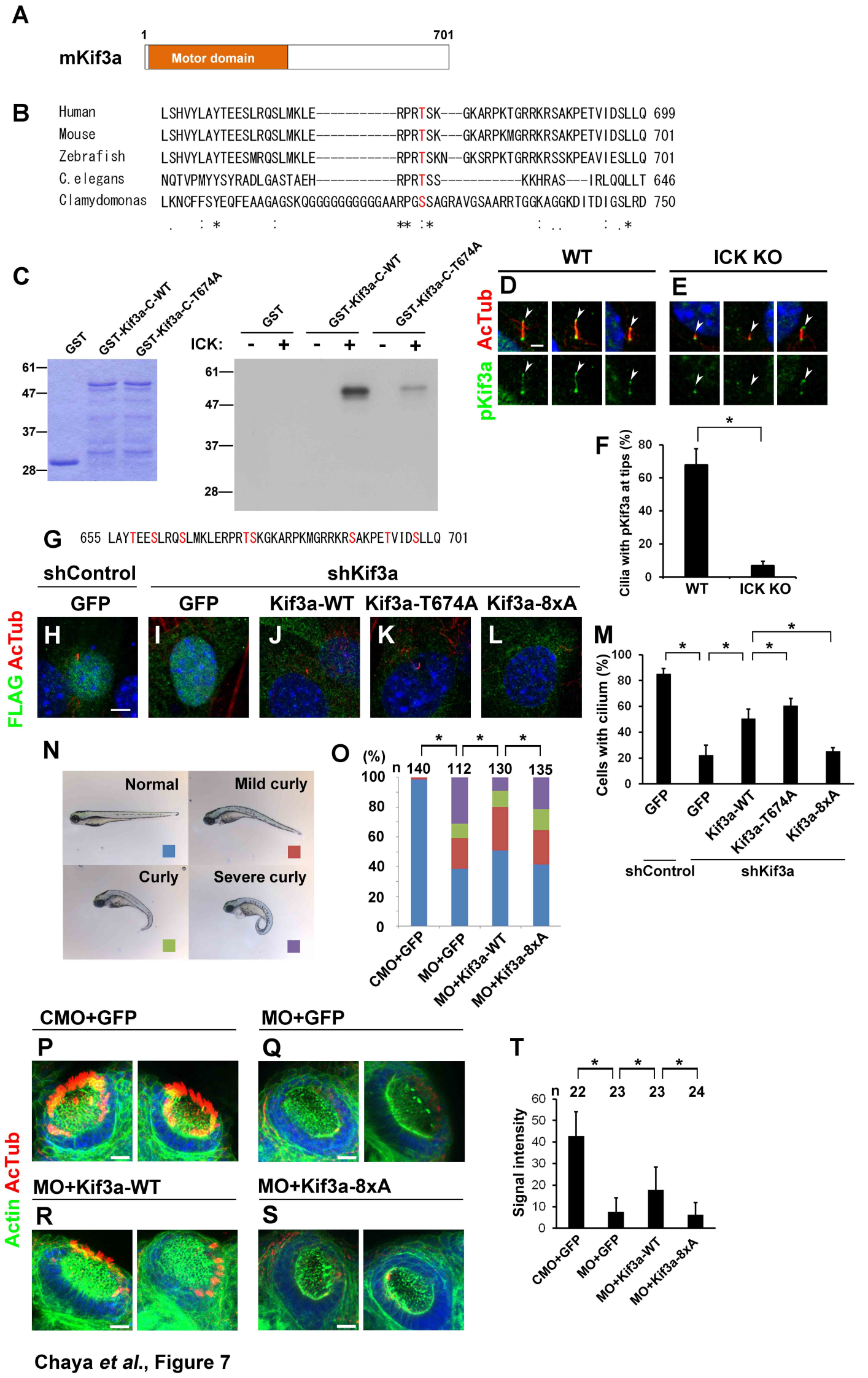

Chaya *et al.*, Figure 7

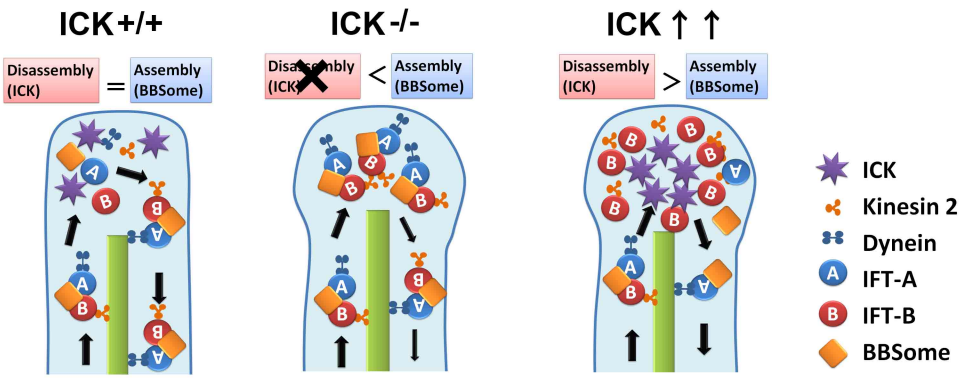

Chaya *et al.*, Figure 8

Supplementary Materials and methods

Animal care

All procedures conformed to the ARVO Statement for the Use of Animals in Ophthalmic and Vision Research, were approved by the Institutional Safety Committee on Recombinant DNA Experiments and the Animal Research Committee of Osaka Bioscience Institute, and by the Recombinant DNA and Animal Experimental Committees of Institute for Protein Research, Osaka University, and were performed in compliance with the Institutional guidelines. Mice were housed in a temperature-controlled room at 22 °C with a 12 h light/dark cycle. Fresh water and rodent diet were available at all times.

In situ hybridization

In situ hybridization was performed as described previously (Muranishi *et al.*, 2011). Digoxigenin-labeled riboprobes for mouse *ICK* were generated by *in vitro* transcription using 11-digoxigenin UTPs (Roche). An *ICK* cDNA fragment for an *in situ* hybridization probe was obtained by PCR using the RIKEN full-length enriched library clone (E130304P20, Genbank accession number AK087484) as a template. The following primers were used: 5'-AAAAATCGATATGAATAGATACACAACGATC AAGC-3' (*ICK-ClaI-F*) and 5'-AAAAGCGGCCGCTCATGATGTAAGGAGGAGGG CCTGTCT-3' (*ICK-NotI-R2*).

Northern blot analysis

Northern blot analysis was performed as described previously (Sanuki *et al.*, 2011).

Total RNAs were extracted from the mouse brain at several developmental stages. Ten micrograms of total RNA were electrophoresed on a 1.0% agarose formaldehyde gel and transferred to a nylon membrane (Pall). The *ICK* cDNA fragment for the *in situ* hybridization probe was used to synthesize radiolabeled probes.

Immunohistochemistry

For immunostaining of the retina, mouse eyes were fixed in 4% paraformaldehyde (PFA) in phosphate-buffered saline (PBS) from 15 s to overnight. For immunostaining of brain sections, brains were fixed by immersion (P4 brains) in 4% PFA in PBS at 4 °C for 16 h or by perfusion (adult brains) in the same fixative. Adult brains were postfixed overnight at 4 °C. For immunostaining of ependymal cilia, brains were not fixed. For immunostaining of E10.5 or E15.5 tissues, embryos were fixed in 4% PFA in PBS for 1h at 4 °C. The tissues were then rinsed in PBS, cryoprotected with 30% sucrose in PBS, embedded in TissueTec OCT compound 4583 (Sakura), frozen, and sectioned. Frozen 20 μm sections on slides were dried for 30 min at room temperature, rehydrated in PBS for 5 min, incubated with blocking buffer (5% normal goat serum, and 0.5% Triton X-100 in PBS) for 1 h, and then with primary antibodies for 4 h at room temperature. Slides were washed with PBS three times for 10 min each time and incubated with secondary antibodies for 2 h at room temperature. The specimens were observed under a laser confocal microscope (LSM700, Carl Zeiss). Zebrafish larvae were fixed in 4% PFA in PBS for 1 h. Whole mount immunostaining of zebrafish larvae was performed using an anti-acetylated α-tubulin antibody (1:2000), phalloidin (1:250), and DAPI as described previously (Omori *et al.*, 2008).

Scanning electron microscopy

For observation of neural tube cilia, samples were washed with PBS, and fixed 1 h on ice with 1% glutaraldehyde in PBS. They were then incubated for 30 min on ice with 1% osmium tetroxide in PBS, dehydrated with ethanol, freeze-dried in t-butyl octanol, and exposed to osmium tetroxide before observation with a scanning electron microscope (S4800, Hitachi).

Immunohistochemical analysis of cilia in the neural tube

Double staining of cilia in the neural tube by antibodies against IFT88 and Arl13b was performed using Zenon Labeling Kit (Lifetechnologies). Each of approximately 1 μg of antibody was labeled with different fluorochromes according to the manufacturer's protocol and used for immunostaining.

Cell culture and transfection

NIH3T3 cells were cultured in DMEM (Sigma) with 10% fetal calf serum and 2 mg/L L-glutamine. Wild-type and *ICK*$^{-/-}$ primary mouse embryonic fibroblasts (MEFs) were generated from embryonic day 13.5 embryos and cultured in DMEM with 10% fetal bovine serum and 2 mg/L L-glutamine. To induce ciliogenesis in MEFs, cells were grown to 80-90% confluency and serum-starved for 48 h. Transfection was performed using Lipofectamine-LTX (Invitrogen) for both NIH3T3 cells and MEFs according to the manufacturer’s instructions. After 24 h, the medium was replaced by serum-free medium. Cells were cultured for from 24 h to 72 h in serum-free medium to induce cilia. For immunostaining, cells were washed with PBS, fixed with 4% PFA in PBS for 5 min at room temperature, and subsequently incubated with blocking buffer for 30

min. Cells were immunostained with a primary antibody in the blocking buffer for 4 h at room temperature and subsequently incubated with the secondary antibody solution for 2 h at room temperature.

***In vitro* kinase assay**

The fusion protein was expressed in *Escherichia coli* strain *DH5a* and purified using glutathione Sepharose 4B (GE healthcare) as previously described (Omori *et al.*, 2010). Purified recombinant GST-tagged full-length human ICK (Abnova) was used for the kinase assay. The kinase reaction was performed with kinase buffer (50 mM HEPES, pH 7.4, 10 mM $MgCl_2$, 5 mM DTT, 20 μM ATP, 10 μCi of [γ-^{32}P]ATP) supplemented with protease inhibitor cocktail (Roche) and phosphatase inhibitor cocktail (Roche) at 30 °C for 60 min. Reaction products were resolved by SDS-PAGE. The gels were dried and exposed to x-ray films.

Injection of antisense morpholino and *in vitro* synthesized mRNA into zebrafish embryos

The breeding and maintenance of zebrafish strains and staging of embryonic development were performed as described previously (Kimmel *et al.*, 1995; Malicki *et al.*, 2002). To rescue morphant phenotypes, Kif3a-WT, Kif3a-CA, and Kif3a-dC were cloned into the *pXT7* vector and transcribed using mMessage mMachine kit (Ambion), according to manufacturer's instructions. 1.0 ng of morpholino and 100 pg of RNA were injected into embryos at the one-cell stage. The morpholino sequence is as follows; Kif3a-ATG, GTTTGTCCAGCTTATTGCTCGGCAT.

Nissl staining

Coronal or sagittal sections from frozen mouse brains were fixed in 4% PFA in PBS for 10 min. After washing in de-ionized water, sections were stained by 0.1% (w/v) cresyl violet for 5 min, washed in 100% ethanol, and incubated in xylene. Slides were coverslipped with Permount (Fisher Scientific).

Antibody production

A cDNA fragment encoding a middle portion of mouse ICK (residues 346-412) was amplified by PCR (Primers: forward 5'-AAAGAATTCCACCCCTACAAAGGCGATG TCTCT-3', reverse 5'-AAAGCGGCCGCTCAAGAACCCTTTGTCGACCTGGAGAT -3'), and subcloned into EcoRI and NotI sites of *pGEX4T-1* (GE Healthcare). The glutathione S-transferase (GST)-tagged fusion protein of ICK was expressed in *Escherichia coli* strain *DH5α* and purified with glutathione sepharose 4B (GE Healthcare). An antiserum against ICK was raised by immunizing guinea pigs with the purified fusion protein (MBL, Nagano, Japan). Then, the antisera were reacted with the fusion protein-coupled CNBr-activated Sepharose 4B (GE healthcare). This sepharose 4B was washed with PBS and eluted with 0.1 M glycine buffer (pH 2.5) to obtain a purified antibody against ICK. The eluted antibody was neutralized by 20 x PBS, and further dialyzed in PBS at 4 °C. An antibody against phosphorylated ($pThr^{674}$) Kif3a was obtained by immunizing rabbits with a phosphorylated peptide ERPRpTSKGKA (MBL, Nagano, Japan).

Staining of the bone and cartilage

Euthanized mice were skinned, eviscerated, and fixed in 95% ethanol for 3-5 days. All specimens were then stained with 0.15% Alcian Blue (Sigma A 3157) dissolved in glacial acetic acid plus 75% ethanol and 0.5% Alizarin Red (Sigma A 5533) dissolved in 2% KOH.

Quantitative real-time PCR (Q-PCR)

Q-PCR was performed using SYBR Green ER Q-PCR Super Mix (Invitrogen) and Thermal Cycler Dice Real Time System Single MRQ TP870 (Takara) according to the manufacturer's protocols. Quantification was performed by Thermal Cycler Dice Real Time System software Ver. 2.0 (Takara). Primer sequences are as follows (Wen *et al.*, 2010) (Omori *et al.*, 2010): for *ICK*, forward (F), 5'-TGGGAAGAATGCATGAACCT TCG-3' (*ICK-Q3*), and reverse (R), 5'-ATGGTCGTTTTCCCTGATAACCTC-3' (*ICK-Q4*); *Gli1*, F, 5'-GCAGTGGGTAACATGAGTGTCT-3 (*Gli1-Q3*), and R, 5'-AG GCACTAGAGTTGAGGAATTGT-3' (*Gli1-Q4*); *Mak*, F, 5'-TATCCAGATGGTGTG CAGAAGAGCC-3′ (*Mak-Q2*) and R, 5'-GAGATGCTGAACTGGGATCCAAAG-3′ (*Mak-P5*); *Ccrk*, F, 5'-CTGGAGGATGGTATTCCT AACCAG-3' (*Ccrk-Q1*), and R, 5'-GGTCCGACAGCATAAATTCGAAAG-3' (*Ccrk-Q2*); *GAPDH*, F, 5'-ACTGGC ATGGCCTTCCGTGTTCCTA-3' (*GAPDH-P1*), and R, 5'-TCAGTGTAGCCCAAGA TGCCCTTC-3' (*GAPDH -P2*).

Western blot analysis

MEFs were washed by PBS twice and lysed in a SDS-sample buffer. P0 retinas and P4 brains were lysed in a lysis buffer (1% Nonidet P-40, 20 mM Tris-HCl (pH 7.4), 150 mM NaCl, and 1 mM EDTA) supplemented with protease inhibitors (1 mM PMSF, 2

μg/ml leupeptin, 5 μg/ml aprotinin, and 3 μg/ml pepstatin A). Samples were resolved by SDS-PAGE and transferred to PVDF membranes. We used the following primary antibodies: mouse monoclonal anti-FLAG-M2 (Sigma, F1804, 1:6000) and anti-α-tubulin (Cell Signaling, DM1A, 1:6000); rabbit polyclonal anti-GFP (MBL, 598, 1:5000); guinea pig polyclonal anti-ICK (1:250) antibodies.

Supplementary References

Kimmel CB, Ballard WW, Kimmel SR, Ullmann B, Schilling TF (1995) Stages of embryonic development of the zebrafish. *Dev Dyn* **203**:253-310

Malicki J, Jo H, Wei X, Hsiung M, Pujic Z (2002) Analysis of gene function in the zebrafish retina. *Methods* **28**:427-438

Muranishi Y, Terada K, Inoue T, Katoh K, Tsujii T, Sanuki R, Kurokawa D, Aizawa S, Tamaki Y, Furukawa T (2011) An essential role for RAX homeoprotein and NOTCH-HES signaling in Otx2 expression in embryonic retinal photoreceptor cell fate determination. *J Neurosci* **31**:16792-16807

Omori Y, Zhao C, Saras A, Mukhopadhyay S, Kim W, Furukawa T, Sengupta P, Veraksa A, Malicki J (2008) Elipsa is an early determinant of ciliogenesis that links the IFT particle to membrane-associated small GTPase Rab8. *Nat Cell Biol* **10**:437-444

Omori Y, Chaya T, Katoh K, Kajimura N, Sato S, Muraoka K, Ueno S, Koyasu T, Kondo M, Furukawa T (2010) Negative regulation of ciliary length by ciliary male germ cell-associated kinase (Mak) is required for retinal photoreceptor survival. *Proc Natl Acad Sci U S A* **107**:22671-22676

Sanuki R, Onishi A, Koike C, Muramatsu R, Watanabe S, Muranishi Y, Irie S, Uneo S, Koyasu T, Matsui R, Cherasse Y, Urade Y, Watanabe D, Kondo M, Yamashita T, Furukawa T (2011) miR-124a is required for hippocampal axogenesis and retinal cone survival through Lhx2 suppression. *Nat Neurosci* **14**:1125-1134

Wen X, Lai CK, Evangelista M, Hongo JA, de Sauvage FJ, Scales SJ (2010) Kinetics of hedgehog-dependent full-length Gli3 accumulation in primary cilia and subsequent degradation. *Mol Cell Biol* **30**:1910-1922

Supplementary Figure legends

Figure S1 Expression of *ICK* and generation of *ICK* floxed mouse line. (**A–E**) *In situ* hybridization analysis of mouse *ICK* in the developing neural tube, brain, and retina. The *ICK* signal was detected in the E10.5 neural tube (**A**) and E15.5 brain (**B**). The *ICK* signal was detected in the developing retina at E17.5, but was not detected at later stages (**C–E**). (**F**) Northern blot analysis of mouse *ICK* in the developing and adult brain. The arrowhead indicates the approximately 6.6-kb *ICK* full-length mRNA. The lower panel shows ethidium bromide staining of the RNA. (**G**) Diagram of the targeting vector, *ICK* flox allele, and *ICK* CKO allele. The yellow boxes, green arrowheads, and red arrowheads indicate exons, *FRT* sites, and *loxP* sites, respectively. Removal of the floxed region by Cre-mediated recombination is predicted to result in a translational frame shift and complete loss of ICK function. (**H**) PCR products of approximately 250 or 400 bp were amplified from the wild-type or targeted allele, respectively. Scale bars, 1 mm (**B**), 500 μm (**A**), and 100 μm (**C–E**). Ctx, cerebral cortex; Str, striatum; NBL, neuroblastic layer; GCL, ganglion cell layer; ONL, outer nuclear layer; INL, inner nuclear layer.

Figure S2 Loss of ICK causes developmental defects. (**A**) *ICK* mRNA expression levels in $ICK^{+/+}$ and $ICK^{-/-}$ MEFs were analyzed by Q-PCR. Error bars show the SD. (**B**) ICK protein expression in $ICK^{+/+}$ and $ICK^{-/-}$ MEFs was examined by Western blot analysis. α-tubulin was used as a loading control. (**C**) *Ccrk* mRNA expression levels in $ICK^{+/+}$ and $ICK^{-/-}$ MEFs were analyzed by Q-PCR. There was no significant difference between $ICK^{+/+}$ and $ICK^{-/-}$ MEFs. (**D**) Dissected lungs from $ICK^{+/+}$

(center), *ICK*$^{+/-}$ (left) and *ICK*$^{-/-}$ (right) embryos. The sizes of the left (red arrowheads) and right (white arrowheads) lobes are substantially smaller in the *ICK*$^{-/-}$ lung. (**E**) The length from top to the bottom of left lobe from *ICK*$^{+/+}$, *ICK*$^{+/-}$ and *ICK*$^{-/-}$ lungs was measured. (**F–H**) Ventral (**F**) and dorsal (**G**) views of brains from E17.5 *ICK*$^{+/+}$ and *ICK*$^{-/-}$ embryos. The olfactory bulbs are conspicuous in the *ICK*$^{+/+}$ brain (arrowhead, left) but not in the *ICK*$^{-/-}$ brain (arrowhead, right). The sagittal length of cerebral cortex (bidirectional arrows) is elongated in *ICK*$^{-/-}$ mice at E17.5 (**G, H**). (**I**) *Gli1* expression in the E15.5 brain from *ICK*$^{+/-}$ and *ICK*$^{-/-}$ embryos was measured by Q-PCR. *Gli1* expression was reduced in the *ICK*$^{-/-}$ brain. (**J–K'**) The cilia in the nasal pit epithelia from *ICK*$^{+/+}$ (**J, J'**) and *ICK*$^{-/-}$ (**K, K'**) mice were stained with the anti-AC3 antibody (red). No obvious difference in the cilia was observed between *ICK*$^{+/+}$ and *ICK*$^{-/-}$ embryos. (**L–Q**) Cilia in the nephric duct lumens (arrowheads in **L, M**), the dermis (Der) and epidermis (ED) of the skin (**N, O**), and muscular layers (LM, longitudinal muscle; CM, circular muscle) and submucosa (Sub) of the intestine (**P, Q**) at E15.5 were stained with an anti-Arl13b antibody (green). Polyglutamylated tubulin (red) was stained to observe the tubulin cytoskeleton in these tissues. Nuclei were stained with DAPI (blue). Scale bars, 2 mm (**D, F, G**), 100 μm (**J, K**), and 10 μm (**J', K', L–Q**). Error bars show the SD. **p* < 0.03. n.s., not significant.

Figure S3 Neural tube patterning of *ICK*$^{-/-}$ embryos and ciliary defects in *ICK*$^{-/-}$ MEFs. (**A–P**) Neural tube patterning of *ICK*$^{-/-}$ embryos. Sections from caudal regions of E10.5 embryos were immunostained with anti-HNF3B (**A, B**), anti-Pax7 (**C, D**), anti-HB9 (**E, F**), anti-Nkx2.2 (**G, H**), anti-Pax6 (**I, J**), anti-Shh (**K, L**), Islet1/2 (**M,**

N), and anti-Nkx6.1 (**O, P**) antibodies. Shh signaling is normal in the neural tube of *ICK*$^{-/-}$ embryos. (**Q–T**) Ciliary defects in the *ICK*$^{-/-}$ neural tube. *ICK*$^{+/+}$ (**Q, Q'**) and *ICK*$^{-/-}$ (**R, R'**) neural tube cilia were immunostained with an antibody against Arl13b. The numbers (**S**) and length (**T**) of the neural tube cilia stained with an anti-Arl13b antibody were measured. The cilia in the *ICK*$^{-/-}$ neural tube are markedly fewer and shorter. (**U–Z**) Ciliary defects in *ICK*$^{-/-}$ MEFs. *ICK*$^{+/+}$ and *ICK*$^{-/-}$ MEFs were immunostained with antibodies against γ-tubulin (a marker for centrioles, red in **U–X**), AC3 (a marker for ciliary membrane, green in **U, V**), and Arl13b (a marker for the ciliary membrane, green in **W, X**). The numbers of the cilia stained with antibodies against AC3 (**Y**), and Arl13b (**Z**) were measured. The cilia in *ICK*$^{-/-}$ MEFs are markedly fewer and shorter. Nuclei were stained with DAPI (blue). Scale bars, 100 μm (**A–P**), 20 μm (left panels in **U–X**), 10 μm (**Q, R**), 2 μm (right panels in **U–X**), and 1 μm (**Q', R'**). Error bars show the SD. **p* < 0.03.

Figure S4 Phenotypic analysis of the *ICK* Dkk3 CKO retina. (**A**) *ICK* mRNA expression levels in the P0 control and *ICK Dkk3* CKO retina were analyzed by Q-PCR. (**B**) ICK protein expression in the P0 control and *ICK Dkk3* CKO retina was examined by Western blot analysis. α-tubulin was used as a loading control. (**C–F**) Immunohistochemical analysis of the *ICK Dkk3* CKO retina at P0. Retinal sections from P0 control and *ICK Dkk3* CKO mice were immunostained with antibodies against cell proliferation markers, Ki67 (green in **C, D**) and PH3 (green in **E, F**). Cell proliferation significantly decreased in the *ICK Dkk3* CKO retina. (**G**) Retinal thickness is reduced in P0 *ICK Dkk3* CKO mice. (**H, I**) The numbers of Ki67-positive cells (**H**) and PH3-positive cells (**I**) in P0 control and *ICK Dkk3* CKO retinas were

counted. (**J–M'**) Photoreceptor cilia were stained with antibodies against acetylated α-tubulin (green in **J–K''**) and Mak (red in **J–K''**) in one month-old control and *ICK Dkk3* CKO mice. Photoreceptor connecting cilia and basal bodies were stained with antibodies against RPGR (red in **L–M'**) and γ-tubulin (green in **L–M'**), respectively. No obvious difference was observed between the control and *ICK Dkk3* CKO retina. (**N, O**) The length of the photoreceptor cilia stained with antibodies against acetylated α-tubulin (**N**) and RPGR (**O**) was measured. There was no significant difference in ciliary length between control and *ICK Dkk3* CKO photoreceptors. Nuclei were stained with DAPI (blue). Scale bars, 100 μm (**C–F**), 5 μm (**J, K, L, M**), and 1 μm (**J', J'', K', K'', L', M'**). Error bars show the SD. **p* < 0.03. n.s., not significant. NBL, neuroblastic layer; GCL, ganglion cell layer.

Figure S5 Phenotypic analysis of *ICK* Nes CKO mice. (**A–D**) *ICK* mRNA expression levels in the P4 control and *ICK Nes* CKO cerebellum (**A**), in the P4 control and *ICK Nes* CKO hippocampus (**B**), in the P4 control and *ICK Nes* CKO cerebral cortex (**C**), and in the P4 control and *ICK Nes* CKO whole brain (**D**) were analyzed by Q-PCR. Error bars show the SD. (**E**) ICK protein expression in the P4 control and *ICK Nes* CKO brain was examined by Western blot analysis. α-tubulin was used as a loading control. (**F**) *Ccrk* mRNA expression levels in the P4 control and *ICK Nes* CKO brain were analyzed by Q-PCR. There was no significant difference between the P4 control and *ICK Nes* CKO brain. (**G**) Growth retardation observed in *ICK Nes* CKO mice (right) compared to control mice (left) at the age of one month. (**H, I**) Nissl staining of sagittal sections from the P21 control (**H**) and *ICK Nes* CKO (**I**) brain. There was no obvious difference in the size of lateral ventricles between the control and *ICK Nes*

CKO brain. (**J, K**) Nissl staining of sagittal cerebellar sections from P4 control (**J**) and *ICK Nes* CKO (**K**) mice. Defects in cerebellar foliation are observed in *ICK Nes* CKO mice. (**L, M**) The numbers of Ki67-positive cells (**L**) and PH3-positive cells (**M**) in control and *ICK Nes* CKO EGL were counted. Ki67-positive cells and PH3-positive cells significantly decreased in *ICK Nes* CKO mice. (**N**) *Gli1* expression was reduced in the *ICK Nes* CKO cerebellum. (**O–T**) Immunohistochemical analysis of the P4 *ICK Nes* CKO hippocampal DG. Sagittal hippocampal sections from P4 control and *ICK Nes* CKO mice were immunostained with antibodies against Ki67 (green in **O, P**) and PH3 (green in **Q, R**). Cell proliferation was decreased in the *ICK Nes* CKO hippocampal DG. The numbers of Ki67-positive cells (**S**) and PH3-positive cells (**T**) in the P4 control and *ICK Nes* CKO hippocampal DG were counted. (**U**) *Gli1* expression in the hippocampus was measured by Q-PCR. (**V, W**) Cilia in ependymal cells are normally formed in the *ICK Nes* CKO brain. Sagittal sections from the P4 control and *ICK Nes* CKO brain were immunostained with an anti-acetylated α-tubulin antibody. (**X–Y'**) Ciliary localization of GPCR in the *ICK Nes* CKO cerebral cortex. Sections from cerebral cortex were stained with ciliary GPCR, SSTR3 (red). The cilia were stained with an anti-AC3 antibody (green). SSTR3 (arrowheads) were localized in the cilia properly both in control and *ICK Nes* CKO mice. Nuclei were stained with DAPI (blue). Scale bars, 20 mm (**G**), 1mm (**H, I**), 500 μm (**J, K**), 200 μm (**O–R**) and 10 μm (**V–Y'**). Error bars show the SD. $^{**}p < 0.03$, $^{*}p < 0.05$, n.s., not significant. LV, lateral ventricle.

Figure S6 Loss of ICK affects ciliary transport. (**A–H**) $ICK^{+/+}$ and $ICK^{-/-}$ MEFs were treated or not treated with Smo agonist (SAG) and immunostained with antibodies

against Smo (green in **A–D**) and Gli2 (red in **E–H**). The cilia were immunostained with an antibody against acetylated α-tubulin (green in **E–H**). Centrioles were immunostained with an antibody against γ-tubulin (red in **A–D**). Smo and Gli2 are aberrantly present in the *ICK*$^{-/-}$ MEF cilia without stimulation with SAG. (**I**) Quantification of the cilia with Gli2 signals. The percentages of the cilia with Gli2 signals in *ICK*$^{+/+}$ and *ICK*$^{-/-}$ MEFs with or without treatment of SAG were quantified. (**J**) Shh signal-dependent expression of *Gli1* is defective in *ICK*$^{-/-}$ MEFs. *ICK*$^{+/+}$ and *ICK*$^{-/-}$ MEFs were untreated or treated with SAG and *Gli1* mRNA expression level was measured by Q-PCR. (**K–N**) FLAG-tagged IFT57- (**K, L**) or IFT140- (**M, N**) expressing plasmids were transfected into *ICK*$^{+/+}$ and *ICK*$^{-/-}$ MEFs. Cells were stained with anti-acetylated α-tubulin (red) and anti-FLAG (green) antibodies. Arrowheads indicate ciliary tips. (**O–P'**) *ICK*$^{+/+}$ (**O, O'**) and *ICK*$^{-/-}$ (**P, P'**) neural tube cilia at E10.5 were immunostained with antibodies against IFT88 (green) and Arl13b (red). There was no obvious difference in ciliary localization of IFT88 between *ICK*$^{+/+}$ and *ICK*$^{-/-}$ neural tube cilia. Arrowheads indicate cilia. Nuclei were stained with DAPI (blue). Scale bars, 2 μm (**A–H, K–N**) and 1 μm (**O–P'**). Error bars show the SD. $^{**}p < 0.03$, $^{*}p < 0.05$.

Figure S7 Characterization of cilia in ICK-overexpressing cells. (**A, B**) The FLAG-tagged construct expressing ICK-WT was transfected into NIH3T3 cells. Cells were stained with anti-ICK (red), anti-acetylated α-tubulin (green), and anti-FLAG (blue) antibodies. ICK signals at ciliary tips increased in FLAG-positive cells. (**C–E**) Overexpression of ICK induced slight ciliary elongation. FLAG-tagged constructs expressing GFP (**C**) or ICK-WT (**D**) were transfected into NIH3T3 cells.

Cells were stained with anti-FLAG (green) and anti-acetylated α-tubulin (red) antibodies. (**E**) The length of cilia stained with anti-acetylated α-tubulin antibody was measured. Arrowheads indicate ciliary tips. Nuclei were stained with DAPI (blue). Scale bars, 5 μm (**C, D**) and 2 μm (**A, B**)

Figure S8 Characterization of an anti-p-Kif3a antibody and a hypothetical model for ICK function. (**A–C'**) The FLAG-tagged GFP- (**A, A'**), ICK-WT- (**B, B'**), or ICK-KD- (**C, C'**) expressing plasmids were transfected into NIH3T3 cells. Cells were stained with anti-FLAG (green) and anti-p-Kif3a (red) antibodies. (**D**) Inhibition test of shRNA expression constructs to knockdown *Kif3a*. Control shRNA or each of three types of shKif3a (shKif3a-1, -2, and -3) expression plasmids was co-transfected with GFP-expressing plasmids and FLAG-tagged Kif3a-WT-expressing constructs into HEK293T cells. Western blotting was performed using an antibody against FLAG. GFP was used as an internal transfection control. All the shRNAs against *Kif3a* showed an inhibitory effect on *Kif3a*. For rescue experiments, shKif3a-1 was used. (**E**) Schematic diagrams representing ICK function in neural progenitor cells and mature neurons. ICK is required for ciliogenesis in neuronal progenitor cells. *ICK*-deficient neural progenitor cells show aberrant accumulation of Smo in the cilia and exhibit a defect of Shh signaling. In contrast, ICK is dispensable for ciliogenesis in mature neurons. Nuclei were stained with DAPI (blue). Scale bar represents 20 μm.

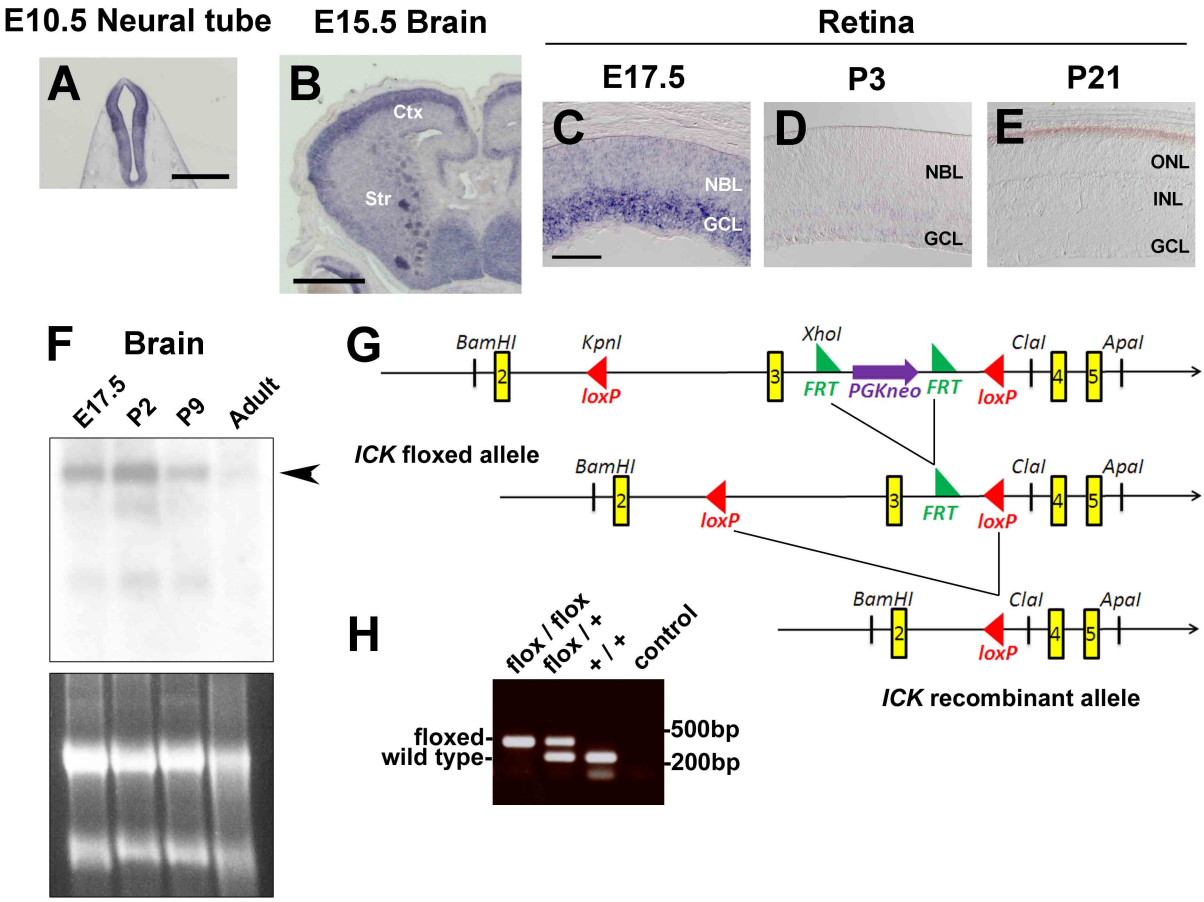

Chaya *et al.*, Figure S1

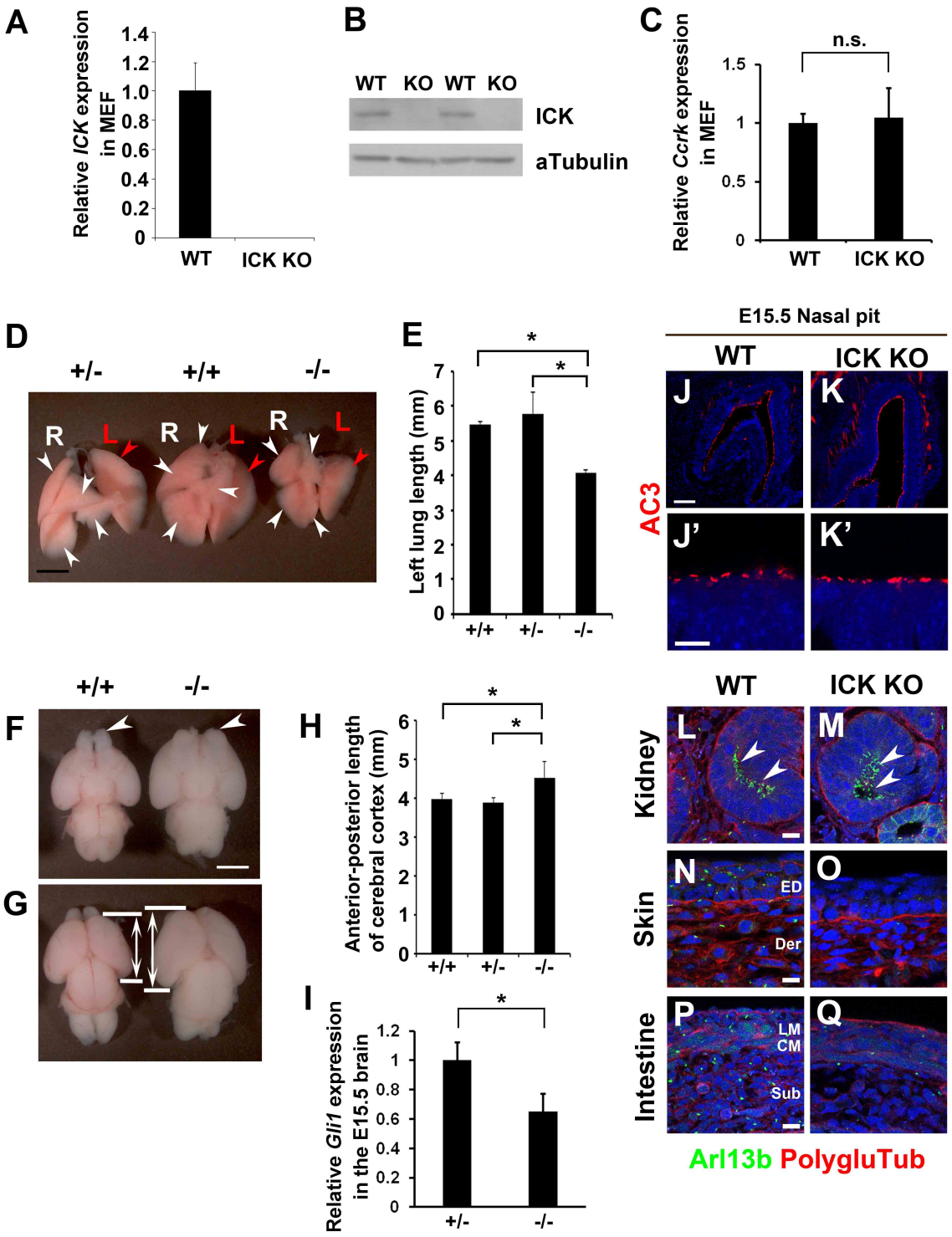

Chaya *et al.*, Figure S2

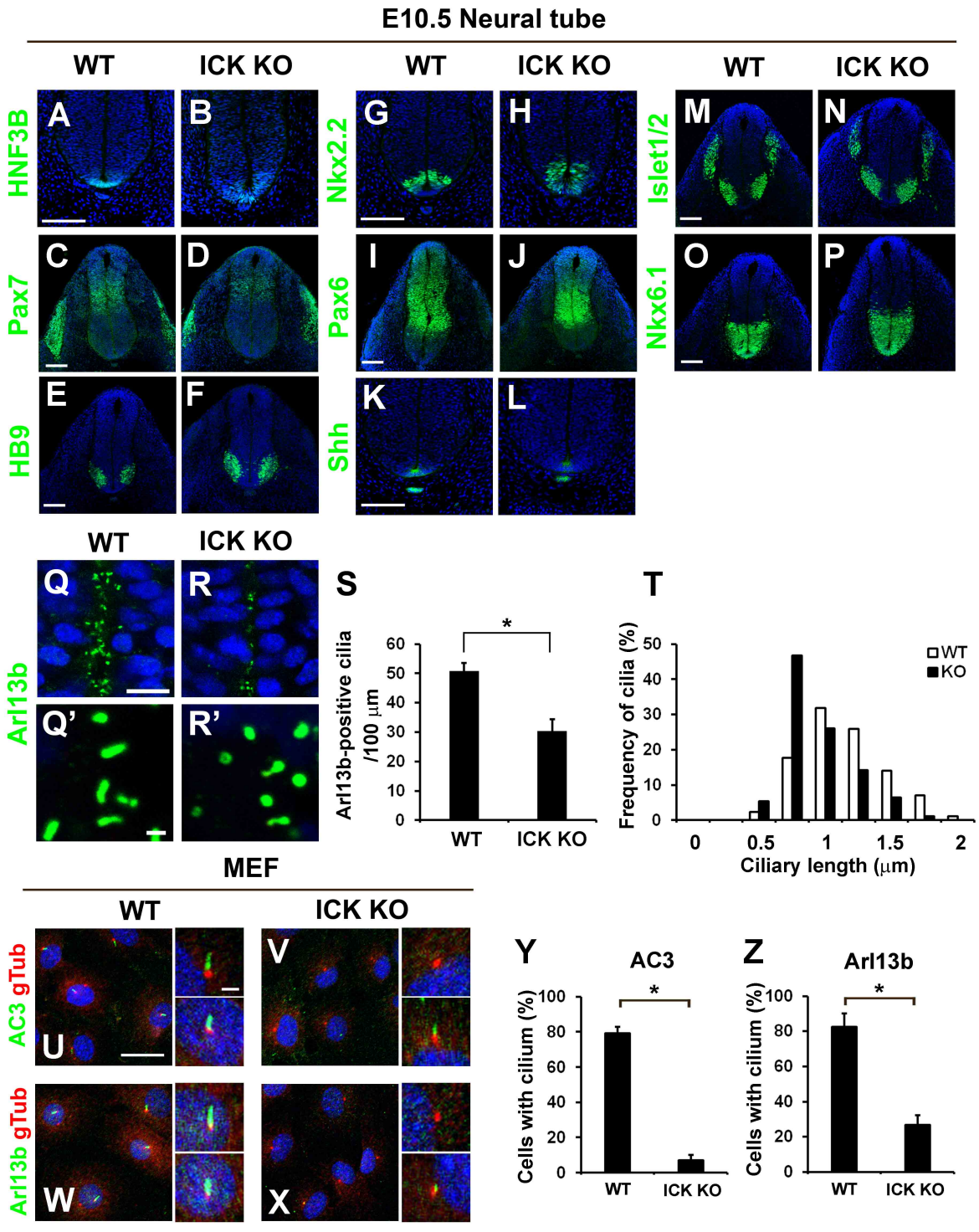

Chaya *et al.*, Figure S3

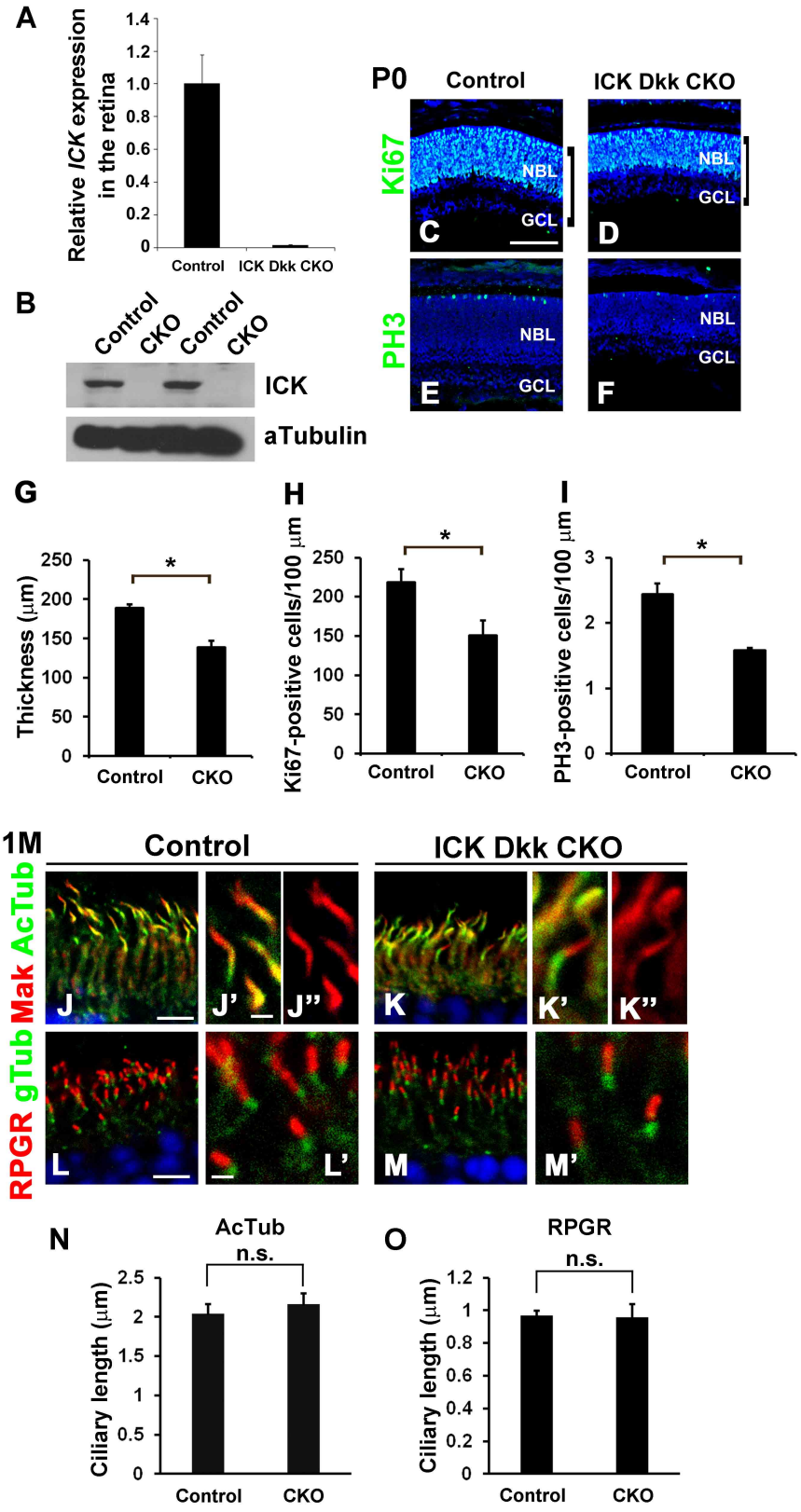

Chaya *et al.*, Figure S4

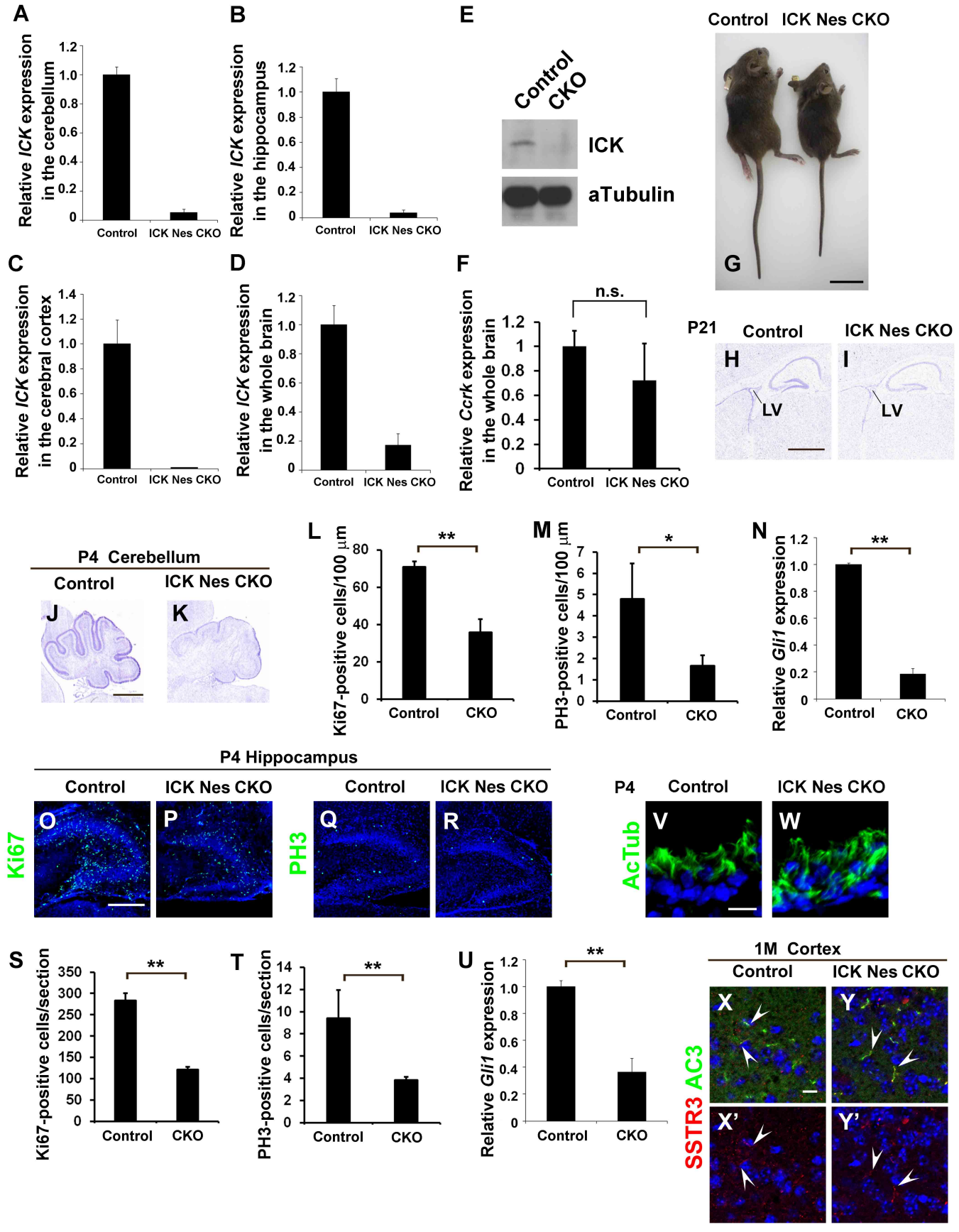

Chaya *et al.*, Figure S5

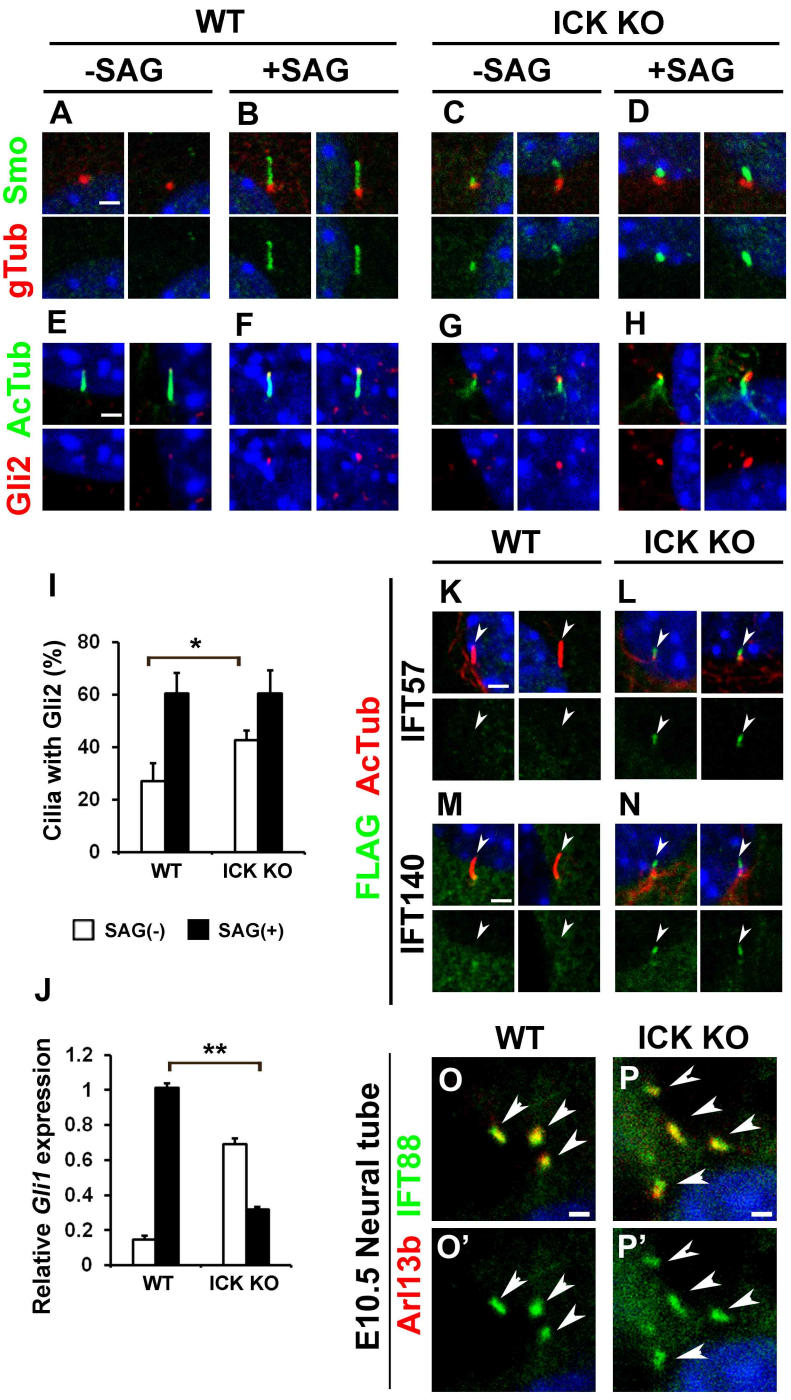

Chaya *et al.*, Figure S6

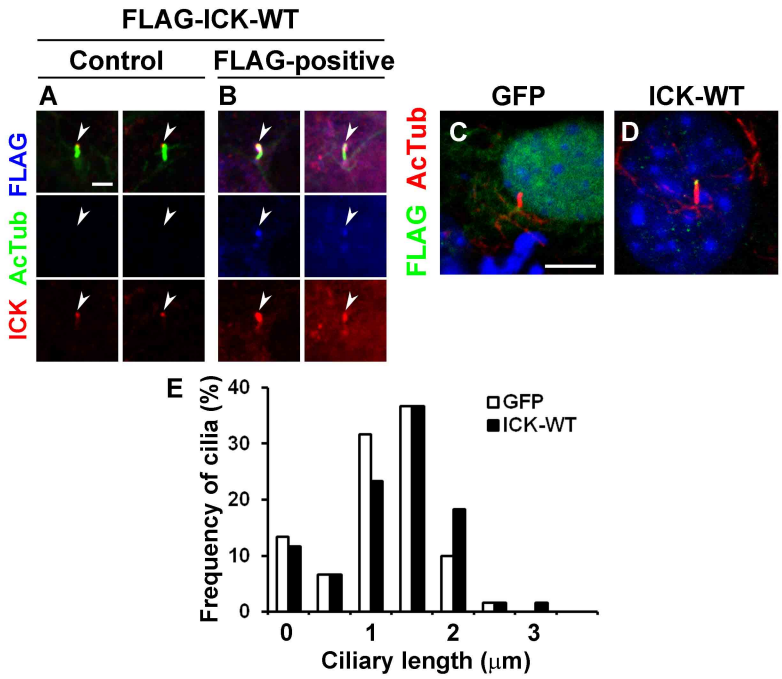

Chaya *et al.*, Figure S7

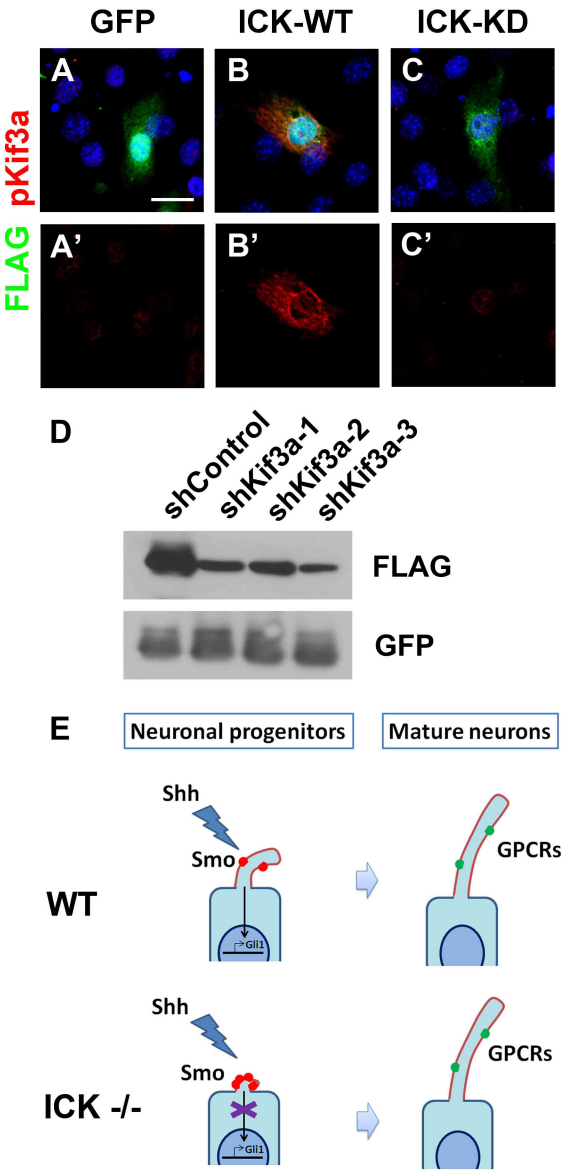

Chaya *et al.*, Figure S8